Open access • Journal Article • DOI:10.1002/2016JD025097

The impact of standard and hard-coded parameters on the hydrologic fluxes in the Noah-MP land surface model — Source link

Matthias Cuntz, Matthias Cuntz, Juliane Mai, Luis Samaniego ...+6 more authors

Institutions: University of Lorraine, Helmholtz Centre for Environmental Research - UFZ, National Center for Atmospheric Research, University of Hohenheim ...+1 more institutions

Published on: 27 Sep 2016 - Journal of Geophysical Research (John Wiley & Sons, Ltd)

Topics: Hydrological modelling, Surface runoff and Water balance

The impact of standard and hard-coded parameters on the hydrologic fluxes in the Noah-MP land surface model

Matthias Cuntz, Juliane Mai, Luis Samaniego, Martyn Clark, Volker Wulfmeyer, Oliver Branch, Sabine Attinger, Stephan Thober

AGU PUBLICATIONS

JGR

Journal of Geophysical Research: Atmospheres

RESEARCH ARTICLE
10.1002/2016JD025097

Key Points:
- Hydrologic fluxes of Noah-MP are sensitive to standard parameters as well as hard-coded values
- Most sensitive model parameter is hard-coded in soil surface resistance for evaporation
- Latent heat and runoff are sensitive to both plant and soil parameters

Correspondence to:
M. Cuntz,
matthias.cuntz@ufz.de

Citation:
Cuntz, M., J. Mai, L. Samaniego, M. Clark, V. Wulfmeyer, O. Branch, S. Attinger, and S. Thober (2016), The impact of standard and hard-coded parameters on the hydrologic fluxes in the Noah-MP land surface model, *J. Geophys. Res. Atmos.*, *121*, 10,676–10,700, doi:10.1002/2016JD025097.

Received 15 MAR 2016
Accepted 7 SEP 2016
Accepted article online 17 SEP 2016
Published online 28 SEP 2016

The impact of standard and hard-coded parameters on the hydrologic fluxes in the Noah-MP land surface model

Matthias Cuntz[1,2], Juliane Mai[1], Luis Samaniego[1], Martyn Clark[3], Volker Wulfmeyer[4], Oliver Branch[4], Sabine Attinger[1,5], and Stephan Thober[1]

[1]Department of Computational Hydrosystems, UFZ-Helmholtz Centre for Environmental Research, Leipzig, Germany, [2]Now at INRA-Université de Lorraine, UMR Ecologie et Ecophysiologie Forestières, Champenoux-Vandoeuvre Les Nancy, France, [3]Research Applications Laboratory, National Center for Atmospheric Research, Boulder, Colorado, USA, [4]Institute of Physics and Meteorology, University of Hohenheim, Stuttgart, Germany, [5]Institute of Geosciences, University of Jena, Jena, Germany

Abstract Land surface models incorporate a large number of process descriptions, containing a multitude of parameters. These parameters are typically read from tabulated input files. Some of these parameters might be fixed numbers in the computer code though, which hinder model agility during calibration. Here we identified 139 hard-coded parameters in the model code of the Noah land surface model with multiple process options (Noah-MP). We performed a Sobol' global sensitivity analysis of Noah-MP for a specific set of process options, which includes 42 out of the 71 standard parameters and 75 out of the 139 hard-coded parameters. The sensitivities of the hydrologic output fluxes latent heat and total runoff as well as their component fluxes were evaluated at 12 catchments within the United States with very different hydrometeorological regimes. Noah-MP's hydrologic output fluxes are sensitive to two thirds of its applicable standard parameters (i.e., Sobol' indexes above 1%). The most sensitive parameter is, however, a hard-coded value in the formulation of soil surface resistance for direct evaporation, which proved to be oversensitive in other land surface models as well. Surface runoff is sensitive to almost all hard-coded parameters of the snow processes and the meteorological inputs. These parameter sensitivities diminish in total runoff. Assessing these parameters in model calibration would require detailed snow observations or the calculation of hydrologic signatures of the runoff data. Latent heat and total runoff exhibit very similar sensitivities because of their tight coupling via the water balance. A calibration of Noah-MP against either of these fluxes should therefore give comparable results. Moreover, these fluxes are sensitive to both plant and soil parameters. Calibrating, for example, only soil parameters hence limit the ability to derive realistic model parameters. It is thus recommended to include the most sensitive hard-coded model parameters that were exposed in this study when calibrating Noah-MP.

1. Introduction

Land surface models calculate the exchanges of radiation, heat, water, and momentum between the terrestrial land and the atmosphere [*Sellers et al.*, 1997]. They build on earlier biogeochemistry or biogeography models, which historically focused on carbon uptake and the spatial distribution of biomes, respectively [e.g., *Running and Coughlan*, 1988; *Prentice et al.*, 1992]. Land surface models have evolved in the last 25 years to both explicitly represent key details of the landscape [*Wood et al.*, 2011; *Bierkens et al.*, 2015] and explicitly represent a remarkable array of physical, chemical, and biological processes [*Fisher et al.*, 2014; *Milly et al.*, 2014; *Clark et al.*, 2015a]. The differences among land surface, biogeochemistry, biogeography, biophysical, and hydrologic models have become less distinct over time, so that land surface models are used in largely different context within different communities such as in assessing the role of vegetation dynamics on climate [*Claussen et al.*, 2013] or in hydrological forecast systems [*Wood and Lettenmaier*, 2006]. All processes represented in current land surface models are, therefore, not equally important for all model outputs and in all regions on Earth. Snow processes might be less important in tropical regions, or microbial turnover times might be less important for net radiation. It is thus an informative step in model development to assess the sensitivity of different model output variables to model parameters in different climatic regions [*Demaria et al.*, 2007; *Van Werkhoven et al.*, 2008].

The parameters in land surface process descriptions represent the mean physical quantities for a model grid cell of hundreds of square kilometers as well as the associated subgrid variability. A recent development in the land surface community are models that allow the user to choose among different descriptions for the same process such as the Noah land surface model with multiple process options (Noah-MP) [*Niu et al.*, 2011; *Yang et al.*, 2011] and Structure for Unifying Multiple Modeling Alternatives (SUMMA) [*Clark et al.*, 2015a, 2015b] where each individual process description comes with its own parameters. A state-of-the-art land surface model thus has a few hundred parameters that can be soil- and plant-type dependent and are typically specified in lookup tables.

It is not necessarily given that all uncertain values in a process description are revealed to the user as parameters. Process descriptions in land surface models have often a strong empirical basis. It depends on the model developer if values in the empirical equations get exposed as adjustable parameters or are embedded as constant values in the model code. This practice can hide large model sensitivities to these "hidden" parameters to an extent that it becomes very difficult to adequately constrain modern land surface models [*Best et al.*, 2015; *Mendoza et al.*, 2015].

Sensitivity analyses are used to understand how perturbations in model parameters affect simulations of dominant physical processes. This is used in parameter estimation efforts for land surface models to focus attention on a reduced set of model parameters [*Rayner et al.*, 2005; *Santaren et al.*, 2007; *Rosolem et al.*, 2012; *Lu et al.*, 2013]. Within the hydrological community, parameter reduction is often achieved through expert knowledge [*Cai et al.*, 2014], but more objective screening techniques exist as well [*Cuntz et al.*, 2015].

The purpose of this paper is to understand how parameter values in a modern land surface model, Noah-MP [*Niu et al.*, 2011], affect simulations of hydrologic fluxes. We consider the entirety of the computer code of the Noah-MP model, identify all fixed ("hard-coded") values, and conduct comprehensive sensitivity analysis of both the hard-coded and adjustable model parameters. The intended outcomes of this research are twofold: first, we seek to inform model developers about interprocess and intraprocess sensitivities, including hard-coded parameters; and second, we seek to increase knowledge of which parameters have the most impact on simulations of hydrologic processes, so as to inform future parameter estimation efforts. We focus on the hydrologic fluxes latent heat and model runoff and their components because this allows us to inform different communities such as the land-atmosphere interactions and the hydrologic community. Sensible heat exhibits similar sensitivities as latent heat in Noah-MP and transpiration as one of the component fluxes of latent heat shows similar sensitivities as photosynthesis. The hydrologic fluxes considered in this study therefore allow to draw general conclusions.

The remainder of this paper is organized as follows. In section 2 we describe Noah-MP and its parameters, the Sobol' method used for sensitivity analysis, and the Noah-MP configurations for 12 river basins across the contiguous United States. In section 3 we present results from the study, providing detailed results for one river basin and summary results for the 12 catchments considered here. In section 4 we provide a discussion of the results, comparing adjustable model parameters with hard-coded model parameters, contrast our results with those from previous studies, and discuss the similarities to the nonhydrologic output fluxes. Finally, in section 5 we present the primary conclusions from this study.

2. Model, Methods, and Setup

2.1. The Noah-MP Model and Its Parameters

The Noah-MP land surface model [*Niu et al.*, 2011] is the successor of the Noah model [*Chen et al.*, 1996; *Chen and Dudhia*, 2001]. It is used as an augmented land surface scheme for the atmospheric Weather Research and Forecasting (WRF) model [*Skamarock et al.*, 2008]. Just like WRF, there are multiple options for land-atmosphere interaction processes in Noah-MP, which users can select [*Barlage et al.*, 2015]. These options include a variety of formulations of processes such as stomatal conductance, runoff generation, snow and soil parameterizations, and radiative transfer in the canopy.

We focus on water fluxes in Noah-MP, which are evapotranspiration (latent heat) and runoff. We also assess the component fluxes soil evaporation and transpiration, which form total evapotranspiration. The latter also includes wet canopy evaporation, which is not included in the component fluxes soil evaporation and transpiration but is rather a small flux compared to the other components. Evapotranspiration and latent heat are normally synonyms for the same flux but expressed in different units. We generically use latent heat in

Table 1. Noah-MP Parameterization Options Selected

Parameterization	Selected
Dynamic vegetation	4 – Monthly LAI from table and green vegetation fraction f_{veg} as annual observed maximum
Stomatal resistance	1 – Ball-Woodrow-Berry [*Ball et al.*, 1987]
Soil moisture reduction for stomatal resistance controlling	1 – Similar to original Noah using soil moisture [*Chen and Dudhia*, 2001]
Runoff	3 – Infiltration-excess surface runoff and free drainage subsurface runoff [*Schaake et al.*, 1996]
Surface exchange coefficient	1 – Monin-Obukhov similarity [*Brutsaert*, 1982]
Supercooled liquid water in frozen soil	1 – General form of freezing-point depression equation [*Niu and Yang*, 2006]
Frozen soil	1 – Hydraulic properties from total soil water and ice [*Niu and Yang*, 2006]
Radiative transfer	1 – Two-stream approximation with crowns and a maximum gap probability depending greenness fraction from the dynamic vegetation option [*Yang and Friedl*, 2003]
Snow albedo	2 – From land surface scheme CLASS [*Verseghy*, 1991]
Partitioning precipitation into rainfall and snowfall	1 – Functional form of *Jordan* [1991]
Lower boundary condition of soil temperature	2 – Fixed lowest soil temperature from input
Soil/snow temperature time scheme	1 – Semi-implicit

the following for easier distinction with evaporation and transpiration. In addition to the surface exchange fluxes, we also asses the component fluxes surface runoff and subsurface runoff, which together represent the total water runoff. The runoff fluxes do not include any river, groundwater, or other storage terms with the parameter option chosen, but they are pure infiltration excess at the surface and free drainage flow at the subsurface.

Noah-MP calculates a closed energy balance and coupled water and carbon cycles. We complement therefore the analysis of the hydrologic fluxes briefly with the analysis of photosynthesis and sensible heat.

We use version 1.6 of Noah-MP driven within the WRF-Hydro framework [*Gochis et al.*, 2013], which allows simple off-line forcing of the land surface model. The parameterization options of Noah-MP were chosen in accordance with the WRF-Hydro framework and are given in Table 1 and explained in *Niu et al.* [2011]. We do not use the surface, subsurface, and channel routing schemes included in WRF-Hydro, because these would overlay the sensitivities of Noah-MP that we are interested in. We also do not use dynamic vegetation, because *Rosero et al.* [2010] have shown that this only spreads the sensitivity to leaf area index (LAI) onto the new dynamic vegetation parameters but mostly via interacting effects with other parameters. Relating sensitivities to process parameters is therefore much clearer without dynamic vegetation.

Noah-MP calculates energy, water, and carbon dioxide fluxes between the biosphere and the atmosphere for different vegetation types, generically called plant functional types (PFT) here. It reads 49 parameters for each PFT from tabulated files. Not all parameters are active in all parameterization options; some parameters are specific to certain options such as the slope of the Ball-Woodrow-Berry stomatal conductance formulation [*Ball et al.*, 1987] in comparison to the minimum stomatal resistance given for Jarvis' [1976] stomata formulation. Table A1 (cf. Appendix A) lists all Noah-MP standard parameters that are active with the parameterization options used in this study (Table 1). Table A2 lists all Noah-MP standard parameters that are not used within the sensitivity analysis. These parameters are either not active with the chosen parameterization options or they are not used within the calculation of the hydrologic fluxes evaluated in this study.

The plant functional types stand on different soil types, which have nine parameters each, given in tabulated files as well. There are another six parameters given in the input files that are the same for all soils such as the soil heat capacity and the soil depth for temperature calculations.

Our chosen options lead therefore to 42 active standard parameters with 5 parameters for all plant and soil types, 9 parameters for each soil type, and 28 additional parameters for each plant functional type (Table A1).

Noah-MP was developed to improve known limitations of the hydrologic cycle within Noah. It simulates canopy and soil processes that are well described by the standard parameters. It does, however, also include a multilayer snow model and frozen ground, as well as other enhancements. It is striking that there are no snow or frozen ground parameters in Noah-MP's standard parameter set (Tables A1 and A2). The original publication of Noah-MP [*Niu et al.*, 2011] involves, however, quite a number of numerical values such as the maximum liquid water content of snow ($\theta_{\mathrm{liqmax},i} = 0.03$ [$\mathrm{m^3\ m^{-3}}$]).

We, therefore, considered the entirety of Noah-MP's model code and identified all fixed (hard-coded) values that are not physical constants such as the freezing point of water (273.15 [K]) or standard gravity (9.80665 [$\mathrm{m\ s^{-2}}$]). We found 139 of these fixed values in Noah-MP, which we call hard-coded parameters from this point onward (Tables A3 and A4). The hard-coded parameters were simply assigned as numbers within the code. For example, the above maximum liquid water content of snow was given in the code as SSi = 0.03 in the first line of the subroutine SNOWH2O. Some of the hard-coded parameters are even given in lookup tables for the different soil types, such as the albedos of wet and dry soils, which would increase the value count even further.

There are, of course, also multiple parameterization options for snow and ice, meaning that not all of these 139 hard-coded parameters are active with the chosen parameterization options (Table 1) and output fluxes. Table A3 lists the 75 active hard-coded parameters with the chosen options and Table A4 lists all the other 64 hard-coded parameters found but not active in this study. Names and descriptions of the hard-coded parameters are sometimes rather vague, because the hard-coded parameters appear often in empirical formulas such as the exponential dependency of snow melt on snow density (MEXP). Hard-coded parameters that calculate a named quantity in Noah-MP have names related to the named quantity such as the three empirical constants CTHKDRY1 – 3, which link soil bulk density with dry soil thermal conductivity THKDRY [cf. *Peters-Lidard et al.*, 1998].

There are overall 42 standard parameters and 75 hard-coded parameters active at each model grid cell in our setup. We have arranged the parameters into categories, representing the process for which the parameters are most important (see Tables A1 – A4 and figures). This is not unambiguous. For example, most processes after snow fall lead to snow melt and would be categorized into "Snow Water" (SnowW). But different processes act differently on snow melt, meaning that all albedo and emissivity related parameters were categorized into "Snow Energy" (SnowE).

2.2. Sensitivity Analysis

A sensitivity analysis is performed on the standard and hard-coded parameters of Noah-MP. A screening step is performed first, following *Cuntz et al.* [2015], to exclude already the most noninformative parameters from the following, computationally expensive, variance-based sensitivity analysis.

The automated sequential screening is based on the Morris Method [*Morris*, 1991] where the parameter space is sampled in forms of trajectories. Several trajectories are sampled at the same time in the original Morris Method before an average screening index is calculated. The sequential screening, on the other hand, samples the trajectories one after another, where each new trajectory is taking into account only parameters, which were not yet identified as informative by previous trajectories. This avoids unnecessary evaluations of the model.

Only informative parameters enter the sensitivity analysis. We perform the sensitivity analysis method of Sobol' [*Sobol'*, 1993] that samples the whole parameter space and then evaluates the variance created in the model output. It decomposes the total variance V in individual variances V_i if only one parameter i is varied and in composite variances if several parameters are varied at once. The total-order Sobol' index S_{Ti} sums all contributions of a parameter i if it is varied individually, together with another parameter, together with two other parameters, until it is varied with all other parameters. This can be rewritten to be the total variance

V without the sum of all variances where all parameters are varied except parameter i, called $V_{\sim i}$ [cf. *Saltelli et al.*, 2008]. The first-order S_i and total-order S_{Ti} Sobol' sensitivity indexes are thus

$$S_i = V_i/V, \tag{1}$$

$$S_{Ti} = 1 - V_{\sim i}/V\,. \tag{2}$$

Sobol' indexes are calculated from variances of single model outputs. Noah-MP's outputs are time series of state variables and fluxes. Sobol' indexes for each time point can thus be calculated. We consider two different ways to create a time-aggregated Sobol' index here:

1. The arithmetic mean of the Sobol' indexes over all time steps, which can be written as

$$\overline{S_i} = \frac{1}{T}\sum_{t=1}^{T} S_i(t) = \frac{1}{T}\sum_{t=1}^{T}\frac{V_i(t)}{V(t)}\,, \tag{3}$$

$$\overline{S_{Ti}} = \frac{1}{T}\sum_{t=1}^{T} S_{Ti}(t) = 1 - \frac{1}{T}\sum_{t=1}^{T}\frac{V_{\sim i}(t)}{V(t)}\,. \tag{4}$$

   Cuntz et al. [2015] argued that the arithmetic mean should be used if one is interested not only in the large values or peaks of a flux or state but also in the low values. We apply this averaging scheme to the runoff fluxes in this study because both high and low flows lead to extreme conditions such as floods and droughts, respectively.
2. The variance-weighted mean of the Sobol' indexes over all time steps, which can be written as

$$\overline{S_i} = \frac{\sum_{t=1}^{T} V(t)S_i(t)}{\sum_{t=1}^{T} V(t)} = \frac{\sum_{t=1}^{T} V_i(t)}{\sum_{t=1}^{T} V(t)}\,, \tag{5}$$

$$\overline{S_{Ti}} = \frac{\sum_{t=1}^{T} V(t)S_{Ti}(t)}{\sum_{t=1}^{T} V(t)} = 1 - \frac{\sum_{t=1}^{T} V_{\sim i}(t)}{\sum_{t=1}^{T} V(t)}. \tag{6}$$

   This averaging scheme will be dominated by Sobol' indexes of time steps having a high variance. *Cuntz et al.* [2015] argued that this is equivalent to using a flux-weighted mean. This is because parameter variations yield larger variances for large fluxes than for small fluxes in most computer models. *Cuntz et al.* [2015], therefore, proposed the total variance as a surrogate for the flux in the weighting procedure, which comes out as case 2 above. This averaging scheme is used in this study for the atmospheric fluxes soil evaporation, transpiration, and latent heat, as well as sensible heat and photosynthesis. This is due to the fact that the atmosphere is more strongly influenced by larger fluxes so that Sobol' indexes during periods of little atmosphere exchange are hence less interesting for these outputs.

Alternative ways to calculate time-aggregated Sobol' indexes are to calculate these from a measure of the output time series, such as the root-mean-square difference between the individual model runs and an average model run. *Cuntz et al.* [2015] have, however, pointed out difficulties in this procedure, and such aggregation schemes are thus not considered here.

In summary, we calculate weighted Sobol' sensitivity indexes $\overline{S_i}$ and $\overline{S_{Ti}}$ (equations (5) and (6)) for the land-atmosphere fluxes evaporation, transpiration, and latent heat, and plain average Sobol' sensitivity indexes (equations (3) and (4)) for the model discharge surface runoff, subsurface runoff, and total runoff. From here we will avoid the use of the overbar and identify the mean indexes generically as S_i and S_{Ti}, independent of the averaging procedure. All parameters are varied in a range of ±20% of their nominal values while assuring parameter constraints such that canopy bottom height (HVB, Table A1) must be below total canopy height (HVT). The parameter ranges are sampled in the form of a multiplier as opposed to actual parameter values, exactly as in *Prihodko et al.* [2008] and *Rosolem et al.* [2012]. The phrase "flux F is sensitive to parameter i" is used to indicate that the output flux F has a large total-order Sobol' index S_{Ti} for the parameter i. The screening step excludes parameters with Sobol' indexes below about 0.1%. We report all sensitivities of the remaining parameters but focus on larger values. We mainly use the term "sensitive" if the Sobol' index is above 1%.

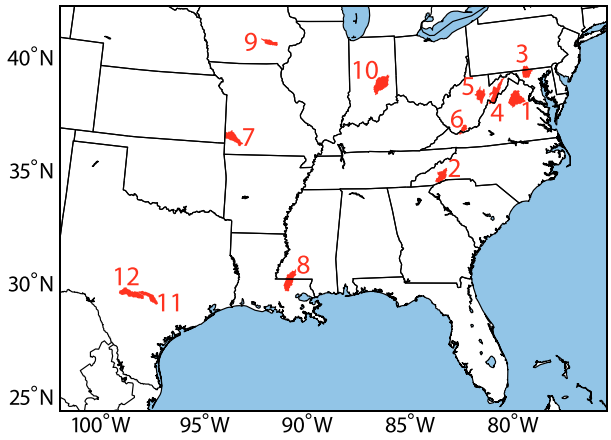

Figure 1. Locations of the 12 MOPEX catchments in the Eastern United States.

2.3. Model Setup at MOPEX Catchments

Noah-MP was setup for 12 catchments in the United States, which represent a wide range of climate envelopes, soil and plant functional types (Figure 1). The catchments were selected during the second phase of the Model Parameter Estimation Experiment (MOPEX). Details can be found in *Duan et al.* [2006].

The hourly meteorological forcing variables were obtained from the North American Land Data Assimilation System project phase 2 (NLDAS-2) data set for the period from 1985 to 2000 at a 1/8° spatial resolution. The NLDAS-2 data set downscales the North American Regional Reanalysis products and additionally assimilates information from different observation-based data sets [*Xia et al.*, 2012]. The land cover and soil textures are also obtained from the NLDAS-2 data set. The former is based on the IGBP-Modis classification using 20 PFTs [*Friedl et al.*, 2010] of which four are no real vegetation but urban builtup, water surfaces, permanent snow and ice, and unvegetated bare soil. The soils are split into 19 texture classes based on the STATSGO soil database [*Miller and White*, 1998].

The spatial location of the 12 catchments is shown in Figure 1, and detailed characteristics can be found in Table 2. With the exception of precipitation and temperature, all of these fluxes have been obtained from a Noah-MP reference run using the default parameter values. Table 2 contains, therefore, mainly model results, but it exposes the importance of each component flux to the total output flux in the model for the individual catchments. The 12 catchments were selected in the second phase of MOPEX for their diverse hydrological characteristics [cf. *Duan et al.*, 2006]. They can be clustered into four groups in terms of vegetation: (1) deciduous forests (catchments 1–7 in Table 2), (2) evergreen forests (catchment 8), (3) cold grasslands (catchments 9 and 10), and (4) warm sparsely vegetated catchments (11 and 12). The deciduous forests have relatively high percentages of snowfall, around 5–15% of total precipitation. Evaporation is higher than transpiration in all of the catchments except for Amite River as well as the first two catchments Rappahannock River and

Table 2. Catchments With Selected Characteristics[a]

#	Name	Soil	Vegetation	P (mm)	S (mm)	T_a (°C)	E (mm)	T (mm)	ET (mm)	Q_{srf} (mm)	Q_{sub} (mm)	Q (mm)
1	Rappahannock River	Silt Loam	Mixed For	1121.7	113.6	12.8	340.3	374.4	784.0	154.4	218.6	373.0
2	French Broad	Loam	Mixed For	1449.6	72.0	12.4	307.6	355.5	753.8	216.0	526.4	742.4
3	Monocacy River	Loam	Decid Broadl For	1122.0	154.0	11.6	383.9	303.9	746.3	142.8	252.2	395.0
4	South Branch Potomac	Silt Loam	Decid Broadl For	1010.5	145.3	10.2	310.2	296.3	674.3	92.5	201.3	293.8
5	Tygart Valley River	Silt Loam	Decid Broadl For	1193.5	139.2	9.7	372.3	273.5	724.7	160.2	337.4	497.6
6	Bluestone River	Silt Loam	Decid Broadl For	918.9	87.9	11.2	335.1	306.4	707.1	80.3	139.6	219.9
7	Spring River	Silt Loam	Decid Broadl For	1177.5	65.8	13.9	456.2	347.5	864.4	187.5	137.3	324.8
8	Amite River	Silt Loam	Evergr Needl For	1641.4	8.0	19.5	335.4	395.4	860.4	323.3	456.9	780.3
9	English River	Silty Clay Loam	Grasslands	966.4	105.0	9.8	617.6	73.5	706.9	211.7	54.7	266.4
10	East Fork White River	Silt Loam	Grasslands	1066.0	87.1	11.6	522.0	211.8	773.6	142.3	156.4	298.7
11	San Marcos River	Clay Loam	Grasslands	909.2	6.1	20.8	390.2	239.7	673.1	210.7	26.7	237.4
12	Guadalupe	Clay	Mosaic	815.2	6.4	19.9	344.9	213.5	597.7	213.7	3.9	217.5

[a]Soil and vegetation are the dominant types in the catchment. Characteristics are annual catchment sums from model output of 1991–2000 except as stated otherwise—P: NLDAS-2 total precipitation, S: snowfall, T_a: NLDAS-2 annual mean air temperature, E: soil evaporation, T: plant transpiration, ET: evapotranspiration, Q: total runoff, Q_{srf}: surface runoff, Q_{sub}: subsurface runoff. Abbreviations in the dominant vegetation types are For = Forest, Decid = Deciduous, Evergr = Evergreen, Broadl = Broadleaf, Needl = Needleleaf.

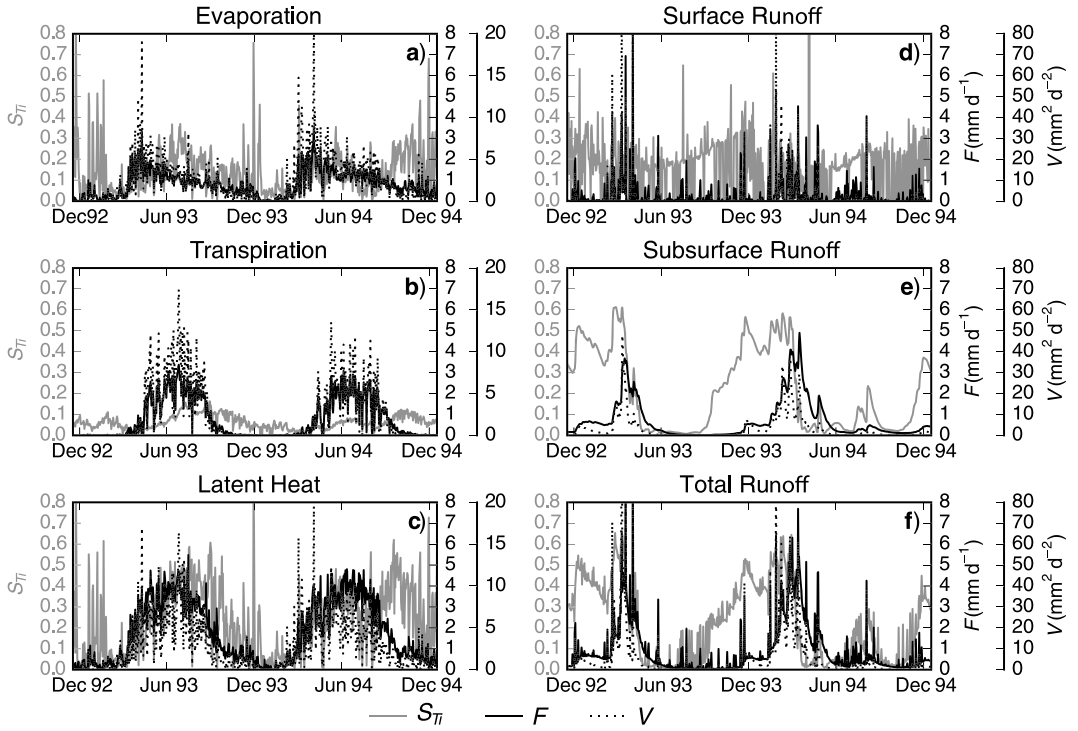

Figure 2. Average fluxes F (solid black lines), total variances V (dotted black lines), and total-order Sobol' sensitivity indexes S_{Ti} (solid gray lines) of the output fluxes (a) evaporation, (b) transpiration, (c) latent heat, (d) surface runoff, (e) subsurface runoff, and (f) total runoff to variations in soil porosity (MAXSMC) at the catchment South Branch Potomac.

French Broad, having also some percentages of evergreen forest. Total runoff consists of two thirds of subsurface runoff and one third of surface runoff in all of these catchments but the Spring River catchment (number 7). Only Amite River has a full evergreen land cover (8 in Table 2). It receives the largest amount of precipitation among all catchments while having only marginal snow fall. It is one of the few catchments where Noah-MP predicts higher annual transpiration than evaporation rates. Subsurface runoff also represents approximately two thirds of the total runoff in Amite River, which seems typical for forested catchments in Noah-MP. Cold grasslands are characterized by very high evaporation rates in comparison to transpiration rates, which is due to very small vegetation fractions of around 42% and low leaf area indexes of at most 2.6 in English River and East Fork White River. Surface runoff fractions are substantially higher in these catchments when compared to the forested ones. The last two sparsely vegetated warm catchments, San Marcos River and Guadalupe, receive the least precipitation among all catchments. They exhibit proportionally low transpiration fractions due to their sparse vegetation, similarly to the other grasslands. The negligible amount of subsurface runoff is the major difference to all other catchments. These dry locations are dominated by moisture-limited conditions, where soil water is much more likely to be transpired than percolate to the bottom of the soil column.

3. Results

3.1. Sobol' Index Time Series for Soil Porosity

Soil porosity, called MAXSMC in Noah-MP, was a consistently informative parameter and mostly a critical parameter for all fluxes in all catchments. Figure 2 shows, therefore, as an example the time series of 2 years of the total-order Sobol' indexes S_{Ti} of MAXSMC for the six output fluxes considered at the snowy catchment South Branch Potomac comprised of mostly deciduous broadleaf forest. Figure 2 shows also the mean fluxes of all parameter sets and their variances for any given time.

Evaporation and transpiration have about the same magnitude in the mean flux (cf. Table 2) but with a different timing in South Branch Potomac. Evaporation increases in spring and decreases gradually during summer when the upper soil dries out. Transpiration starts increasing later in spring and decreases only at the end of summer, following closely seasonal radiation input.

The Sobol' indexes (gray solid lines in Figure 2) have different responses in time than the fluxes (black solid lines in Figure 2). There is not yet much sensitivity to porosity in the formulation of evaporation at the beginning of spring, when the soil is wet. The sensitivity increases with decreasing soil moisture up to a point when the soil is so dry that evaporation gets much reduced independent of the maximum water holding capacity. Evaporation can exhibit very large sensitivities to porosity in winter when evaporation is very little. This is because Sobol's sensitivity indexes are the ratio of two variances, which are both small in winter and vary largely in between the different parameter sets, meaning that the Sobol' indexes have very large error bars (not shown).

Transpiration shows little sensitivity toward porosity in spring and early summer but larger sensitivities in autumn. Porosity is acting on transpiration only via soil moisture limitation of stomatal conductance below a critical soil moisture (REFSMC). So there is only direct sensitivity of transpiration to porosity if soil moisture is restricting stomatal conductance. There are indirect sensitivities at other times due to canopy temperature effects, for example. Notably, there is sensitivity to transpiration when there are no leaves but there is a small fraction of evergreen conifers in South Branch Potomac which transpires the whole year round (if not covered fully by snow).

The different timings of evaporation and transpiration and their respective sensitivity indexes lead to surprising results in the combined flux latent heat. The latent heat flux and its Sobol' index S_{Ti} change are much more in phase. The large transpiration flux weights the sensitivities of evaporation in spring and summer while evaporation weights the larger sensitivities of transpiration in autumn, leading to a double-peak appearance in latent heat Sobol' sensitivity indexes and to values larger for the individual fluxes.

The picture is quite different for the discharge fluxes (Figures 2d – 2f). Surface runoff is calculated as infiltration excess in Noah-MP so that it appears only during periods of rain and shortly after, as well as during snow melt. There are many days when surface runoff is zero, and the sensitivity indexes are set to zero in those cases. Subsurface runoff in the chosen Noah-MP option is the amount of water that drains out of the soil column, for which the lower boundary has a depth of 2 m in Noah-MP. South Branch Potomac never dries out to less than 0.01 $m^3\ m^{-3}$ in the lowest soil layer so that there is always little drainage and therefore subsurface runoff. Both runoffs, surface and subsurface, have the same timing in Noah-MP: if there is rain wetting the soil, there is more infiltration excess but also more soil moisture for subsurface runoff. Total runoff, the sum of surface and subsurface runoff, has thus the same timing as the two component fluxes.

Surface runoff shows a large number of days with no sensitivity because there is no surface runoff. It also shows only a slight seasonality during times having nonzero Sobol' indexes with more sensitivity in midwinter and less sensitivity in summer because infiltration depends on saturation fraction, which itself depends on current soil moisture. Subsurface runoff has high sensitivity in autumn and winter, which ends abruptly just after snow melt. The Sobol' indexes of total runoff resemble the indexes of subsurface runoff with only small variations from surface runoff but with a much reduced value than for the component surface runoff.

Figure 2 shows the variance on top of the output fluxes and confirms that variance is a good surrogate for the mean flux in a weighting procedure.

3.2. Parameter Sensitivities at South Branch Potomac

The time-averaged first and total-order Sobol' indexes S_i and S_{Ti} are shown for all model outputs at the catchment South Branch Potomac in Figure 3. The stacked bar chart has the parameter numbers as given in the first columns of Tables A1 and A3 on the azimuth. Variable names are given in the table but can also be read from the *x* axis of Figure 4. The radius, i.e., the bar heights, are the sensitivity indexes where the darker lower parts are the first-order effects S_i and the total bar heights are the total effects S_{Ti}. The colored top part of the radius are the categories as given in Tables A1 – A4, which are only for ordering the parameters with respect to their main appertaining process. The automated screening procedure was applied before the sensitivity analysis for each output flux independently. Retained parameters are indicated by black circles. Parameters without black dots do not have Sobol' indexes calculated but are given for better comparison between the different output fluxes.

Almost all standard parameters of Noah-MP were screened as being informative for the land-atmosphere fluxes evaporation, transpiration, and latent heat. Only about a third of them have sensitivity indexes above 1% (0.01) for the land-atmosphere fluxes though.

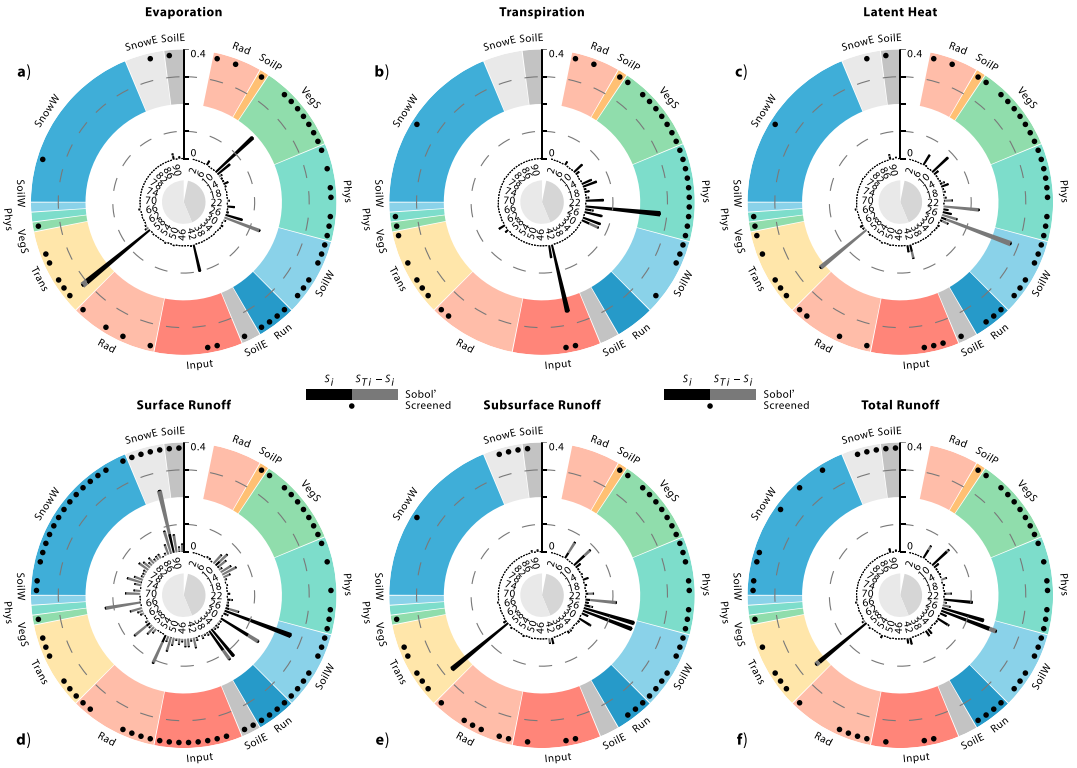

Figure 3. Stacked bar charts of mean first-order and total-order Sobol' indexes S_i and S_{Ti} of standard (Table A1) and hard-coded parameters (Table A3) of the output fluxes (a) evaporation, (b) transpiration, (c) latent heat, (d) surface runoff, (e) subsurface runoff, and (f) total runoff at the catchment South Branch Potomac. The lower gray bars of the stacks are S_i and total stacks are S_{Ti}. Sobol' indexes are variance-weighted averages in time for Figures 3a–3c and plain averages for Figures 3d–3f. Only parameters with a filled circle on top of the radius have Sobol' indexes; all other parameters have a thin horizontal line on the azimuth for visual identification. Colored sections are categories given in the tables. Gray slices in the center indicate the 39 active standard parameters (dark gray, Table A1) and 54 active hard-coded parameters (light gray, Table A3).

The most sensitive standard parameter for evaporation is vegetation height (parameter 10, named HVT in the model code) due to two effects: first, interception depends on vegetation density, which is a function of vegetation height, and second, there is less below-canopy evaporation in higher stands. The second largest sensitivity of the standard parameters is soil porosity (27 MAXSMC) due to the dependence of evaporation on top layer soil moisture. The largest sensitivity of evaporation is due to the hard-coded parameter KRSURF1 (59). This parameter controls the concavity of the dependence of soil dry layer thickness on saturation after *Sakaguchi and Zeng* [2009]. *Sakaguchi and Zeng* compared the original formulation with their new formulation of the resistance for water vapor from the evaporating front in the soil to the top of the soil surface in the Community Land Model (CLM3.5) [from *Sellers et al.*, 1992]. The new formulation had very similar characteristics to the original CLM3.5 version, and the parameter sensitivities show consequently a similarly large dependence of evaporation on this pertaining parameter, as found for the correspondent parameter in CLM3.5 [*Göhler et al.*, 2013].

The slope (23 MP) of the Ball-Woodrow-Berry stomatal conductance model [*Ball et al.*, 1987] exhibits by far the largest sensitivity of the standard parameters for transpiration. Other parameters contributing to the variance in transpiration include structural parameters such as leaf area index (15 LAIM) and physiological parameters such as the maximal carboxylation rate (21 VCMX25) as well as soil parameters such as porosity (27 MAXSMC). They all act differently on transpiration. Leaf area index (LAI) acts on the partitioning of radiation between plant and soil (gap probability), the maximum carboxylation rate changes assimilation, and therefore stomatal conductance (via the Ball-Woodrow-Berry model) and the soil parameters change the limitation of stomatal conductance with soil moisture. Another large sensitivity is found for a hard-coded parameter controlling the division of incoming radiation into direct and diffuse radiation (42 FDIRRAD). This has large influence on the partitioning of evaporation versus transpiration. Transpiration shows also dependence on the division

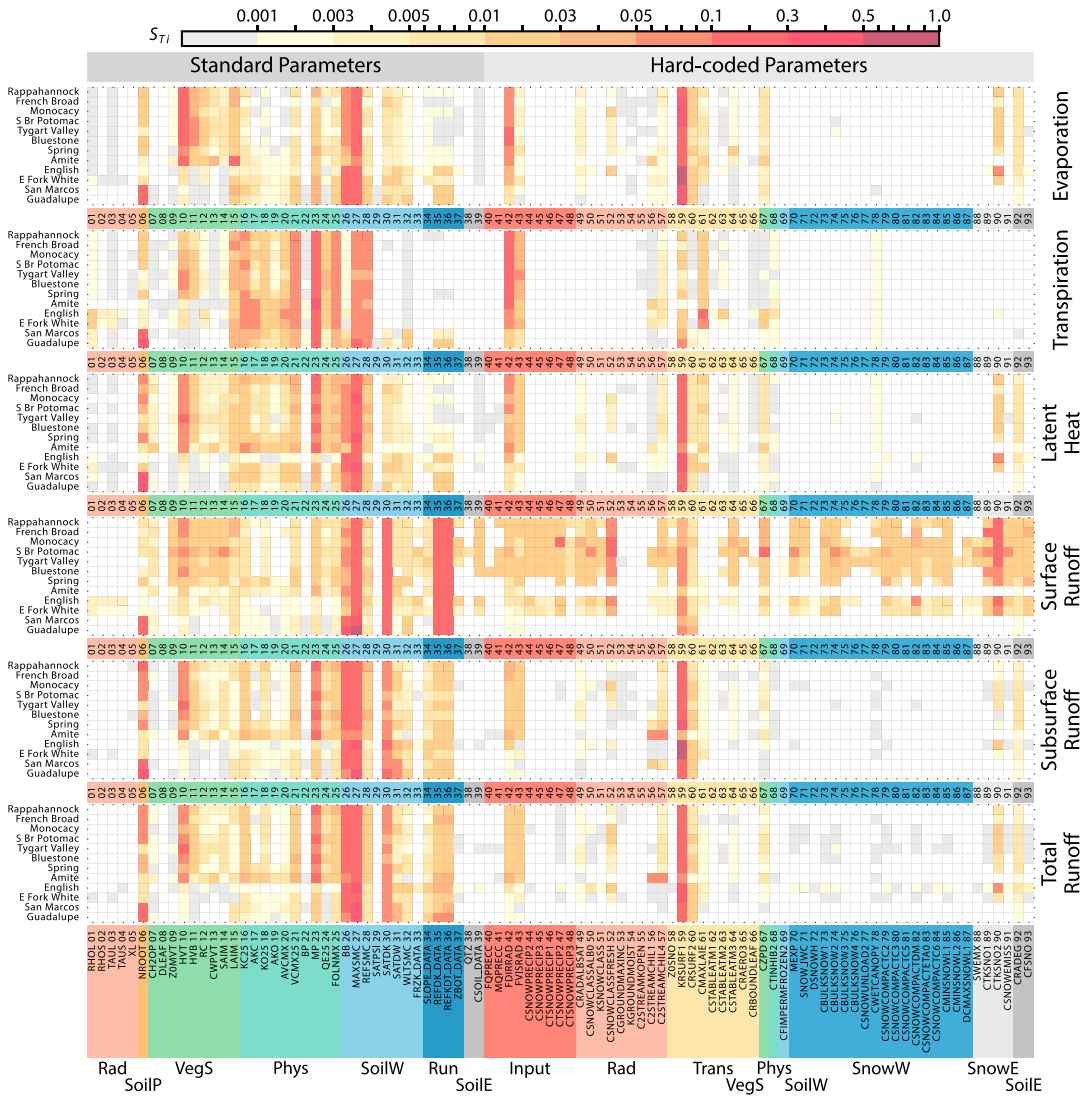

Figure 4. Total-order Sobol' indexes S_{Ti} of standard (Table A1) and hard-coded parameters (Table A3) of the output fluxes evaporation, transpiration, latent heat, surface runoff, subsurface runoff, and total runoff at all 12 MOPEX catchments. Sobol' indexes are variance-weighted averages in time for evaporation, transpiration, and latent heat, and plain averages for surface runoff, subsurface runoff, and total runoff. Note the logarithmic scale of the color bar. Empty cells are parameters that were filtered out during initial parameter screening and no Sobol' index was calculated. Colored sections underlying parameter numbers and names are categories given in the tables.

of incoming solar radiation into visible and near infrared (43 FVISRAD), because this determines how much energy is available for assimilation.

Transpiration fraction is about 44% in South Branch Potomac so that quite a few parameters have hence sensitivities for latent heat that are between those for transpiration and those for evaporation. But some parameters can also exhibit enhanced sensitivities as discussed for soil porosity (27 MAXSMC) in section 3.1. Sensitivities also change from direct effects on the component fluxes to more indirect or interactive effects on the composite flux. For example, the slope of the stomatal conductance formulation (23 MP) directly influences transpiration. The effect on evaporation is only indirect through changed water contents in the top soil layer. The sensitivity for latent heat shows large interaction effects $S_{Ti} - S_i$ because of the strong covariance between evaporation and transpiration. The surface resistance parameter KRSURF1 (59) and the fraction of visible radiation FVISRAD (43) have values for latent heat that are averages between the sensitivities of evaporation and transpiration. KRSURF1 (59) changed from direct effect on evaporation to interaction effects on latent heat due to the same argument as for the slope of the stomatal conductance (23 MP). The sensitivity

of the partitioning of direct and diffuse radiation FDIRRAD (42) almost vanishes for latent heat, showcasing that sensitivities of composite fluxes are not simple weighted averages of the sensitivities of the component fluxes. FDIRRAD (42) influences how deep radiation can penetrate into the canopy which partitions energy between evaporation and transpiration. Latent heat is, however, only little affected because an increase in transpiration thus implies a decrease in evaporation and vice versa.

There are 14 Noah-MP standard parameters with sensitivity indexes above 1% for surface runoff, which is calculated as pure infiltration excess with the chosen parameterization option (Table 1). The soil water and runoff parameters are hence linked to the calculation of the saturated area in a grid cell (e.g., 27 MAXSMC, 35 REFDK_DATA, 36 REFKDT_DATA) or to the speed at which water can be transported away from the surface, i.e., the hydraulic conductivity (30 SATDK). Vegetation structure is also important for surface runoff because it regulates snow and rain interception by the canopy. The number of sensitive (>1%) hard-coded parameters in surface runoff is striking. Surface runoff has by far the most informative and sensitive parameters from all analyzed output fluxes. There are two very sensitive hard-coded snow parameters in surface runoff. These are the exponential dependence of snow thermal conductivity on snow density (90 CTKSNO2) and the albedo of fresh snow in the CLASS snow scheme (52 CSNOWCLASSFRESH). All other (hard-coded) snow parameters also show notable sensitivities, which are dominated by interacting effects. This indicates that they might well affect each other. Quite a few parameters influence snow processes, although they are not linked to snow at first sight. For example, the ratio of displacement to vegetation height (67 CZPD), which exhibits the second largest sensitivity, interacts largely with vegetation height but also impacts snow interception. Another example are the two parameters correcting aerodynamic resistances in stable and unstable conditions (63 CSTABLEATM2, 64 CSTABLEATM3) that also influence heat transport to and from the snow pack and hence snow melt.

There are surprisingly no runoff parameters (34–37) important for subsurface runoff. Subsurface runoff, being soil drainage with the chosen option, comes from the same reservoir as latent heat, i.e., soil moisture. Similar parameters as for latent heat are hence sensitive, like soil porosity (27 MAXSMC), the slope of stomatal conductance (23 MP), or the hard-coded surface resistance parameter KRSURF1 (59), which has the overall largest sensitivity. There is one additional standard parameter sensitive in subsurface runoff compared to latent heat due to different timings, because the drainage of wet soils is independent of atmospheric conditions. This is the Brooks-Corey parameter (26 BB) for the relation between soil moisture and matric potential, which is also used in the dependence of hydraulic conductivity on soil moisture [*Brooks and Corey*, 1964]. Subsurface runoff would be sensitive to groundwater parameters such as the "baseflow coefficient" in other runoff options than the one chosen. But groundwater mostly acts as a low-pass filter in Noah-MP so that these options would have disguised the strong link between latent heat and discharge.

Total runoff is dominated by subsurface runoff in the catchment South Branch Potomac (Table 2). The sensitivities of total runoff to the Noah-MP standard parameter therefore resemble closely the sensitivities of subsurface runoff and thus also latent heat. Snow parameters are almost not visible anymore with very little remnant of snow thermal conductivity (90 CTKSNO2). This is not only due to the dominance of subsurface runoff but also because surface runoff from snow melt is active only at a few time steps and zero at other times in the chosen configuration. Any influence of snow parameters on total runoff is hence much diluted.

3.3. Parameter Sensitivities at 12 MOPEX Catchments

At all 12 MOPEX catchments, Sobol' indexes were calculated for the chosen model output fluxes and averaged in time differently for the land-atmosphere fluxes and runoff, as discussed before. Figure 4 summarizes the results for the total-order Sobol' indexes S_{Ti}. Each line is basically an unfolded version of one radial plot in Figure 3 where the colors correspond to total bar height. For example, the fourth line for evaporation in Figure 4 are the same results as in Figure 3a. Gray squares represent parameters where variations of the parameters lead to less than 0.1% variation in the output flux. No Sobol' indexes were calculated for unfilled squares, which were filtered out during the initial automated sequential screening [*Cuntz et al.*, 2015]. The screening is hence so conservative that it keeps parameters that cause less than 0.1% variation in output but still filters out three quarters of all parameters except for surface runoff, where about half of the parameters are kept for the sensitivity analysis. Sensitivity indexes would be about 1% in our case if all parameters were contributing equally to the output variability. A more realistic scenario would probably deem a parameter sensitive if its total-order Sobol' index is above 0.5%.

The catchments are sorted as in Table 2 with forested catchments on top and grasslands on the bottom. The last two catchments are in Texas having a hot climate with average precipitation. The five MOPEX catchments Monocacy River, South Branch Potomac, Tygart Valley River, Bluestone River, and Spring River (3–7 in Table 2) have similar vegetation and climate. Amite River (8) experiences a humid subtropical climate, although it has mostly coniferous forest. It represents alone, though, warm evergreen forests, competing visually against five temperate deciduous broadleaf forests.

The figure shows vertical lines of highly sensitive parameters, which means that these parameters are sensitive in all catchments. Especially soil porosity (27 MAXSMC) is sensitive in all catchments for each output flux with all total-order Sobol' indexes S_{Ti} above 5%. This means that at least 5% of total model variability observed with all parameter sets comes from variation of soil porosity alone and in combination with other parameters. The Brooks-Corey parameter (26 BB) and the hard-coded surface resistance parameter (59 KRSURF1) are also sensitive in all catchments and for all fluxes except transpiration and surface runoff. Both parameters regulate how fast water can be removed from the first soil layer either by percolation (BB) or by evaporation (KRSURF1). The sensitivities of all other parameters depend more on basin characteristics and individual fluxes such as the two runoff parameters (35 REFDK_DATA, 36 REFKDT_DATA), which are important only for surface runoff because they influence the saturated area of a grid cell.

The land-atmosphere fluxes evaporation, transpiration, and latent heat have a couple of parameters that are sensitive in all catchments but of different magnitudes. Evaporation displays coherent sensitivity only to the three parameters above (i.e., 26 BB, 27 MAXSMC, and 59 KRSURF1) while transpiration shows also systematic sensitivity to almost all physiology parameters (category Phys) such as carboxylation efficiency (21 VCMX25). The Brooks-Corey parameter (26 BB) is less sensitive for transpiration, but reference saturation (28 REFSMC) is becoming sensitive (>5%) for transpiration, below which there is water limitation of stomatal conductance. The land-atmosphere fluxes present a division between forested (top 8) and grassland (lower 4) river catchments in other categories such as vegetation structure parameters (category VegS) like vegetation height (10 HVT). Grassland ecosystems show expectedly almost no sensitivity to vegetation structure parameters. This division can also be seen in the hard-coded input parameter that partitions direct and diffuse radiation (42 FDIRRAD). Diffuse radiation can penetrate deeper into the canopy, increasing production and transpiration in the light-limited part of the canopy, as well as increasing the amount of energy reaching the forest floor. This is more important the more vegetation there is. Grasslands have less vegetation density in Noah-MP and are hence less sensitive to the type of radiation, i.e., FDIRRAD (42). The parameter for the number of soil layers with roots (06 NROOT) stands out for the land-atmosphere fluxes at the two Texas catchments, San Marcos River and Guadalupe. Root density does influence the availability of water for the vegetation, but it also influences the amount of available water for abiotic extraction. It is hence sensitive (>1%) in all three atmosphere fluxes and is even larger for latent heat than for the component fluxes evaporation and transpiration individually. The catchment South Branch Potomac of Figures 2 and 3 can be regarded as an intermediate catchment for deciduous forests within the MOPEX catchments with respect to its parameter sensitivities; i.e., it does not exhibit substantially more or less parameters with sensitivities above 1% than the average number across all catchments.

Soil porosity (27 MAXSMC), saturated hydraulic conductivity (30 SATDK), and the runoff parameters (35 REFDK_DATA, 36 REFKDT_DATA) are consistently sensitive for surface runoff in all catchments. Among all fluxes, hard-coded snow parameters are the most sensitive for surface runoff. There are differences between the catchments but their Sobol' indexes S_{Ti} alternate mostly between 1% and 5%. Some hard-coded snow parameters stand out, particularly the snow thermal conductivity (90 CTKSNO2) and its limit for very fluffy fresh snow (89 CTKSNO1) as well as the albedo of fresh snow (52 CSNOWCLASSFRESH). These parameters act on the snow energy budget rather than the snow texture such as bulk density. Snow textural parameters (category SnowW) are, however, almost all sensitive with Sobol' indexes from 1% to 5%, which are higher for forest than for snowy catchments (i.e., English River, East Fork White River). The latter exhibit little sensitivity in almost all parameters but are dominated by a few highly sensitive parameters.

Subsurface runoff shows similar sensitivities as the land-atmosphere fluxes with the three most sensitive parameters being BB (26), MAXSMC (27), and KRSURF1 (59). Additionally, the saturated hydraulic conductivity (30 SATDK) becomes sensitive (>5%), because subsurface runoff is purely soil drainage in the chosen parameterization option (Table 1). Sensitivities for subsurface runoff also exhibit the division between forested and grassland catchments especially for vegetation structure parameters (category VegS). Two parameters

from the radiation scheme are sensitive (>5%) in the evergreen forest-dominated catchment Amite River (56 C2STREAMCHIL1, 57 C2STREAMCHIL4). The two parameters are used in the calculation of absorbed radiation depending on leaf angle distribution given by leaf angle parameter XL (5), which means that subsurface runoff is also sensitive to the distribution of energy between soil and canopy. Total runoff resembles subsurface runoff in all catchments as seen previously for South Branch Potomac.

4. Discussion

A comprehensive sensitivity analysis for the Noah land surface model with multiple process options (Noah-MP) is presented here. The original Noah [*Chen et al.*, 1996; *Chen and Dudhia*, 2001] has been used and studied as an off-line model and as the land surface component of regional weather models [cf. *Ek et al.*, 2003, and references therein]. Noah has only a primitive vegetation model and calculates latent heat as potential evapotranspiration based on Penman-Monteith, which is reduced in case of limited soil moisture. Noah-MP on the other hand has a state-of-the-art vegetation description with a coupled photosynthesis-stomatal conductance scheme including sophisticated descriptions of canopy micrometeorology. It is therefore difficult to compare results for Noah [e.g., *Rosero et al.*, 2010] with our results for Noah-MP. The hydrology of Noah-MP was, however, subject of several studies, for example, *Cai et al.* [2014], *Barlage et al.* [2015], and *Mendoza et al.* [2015].

4.1. Soil and Vegetation Parameters

Cai et al. [2014] performed a sensitivity analysis of total runoff on the three parameters: soil porosity (27 MAXSMC), saturated hydraulic conductivity (30 SATDK), and already on the hard-coded surface resistance parameter (59 KRSURF1), which they called "surface dryness factor" (α). They were chosen "based on modeling experience and previous studies" [*Cai et al.*, 2014]. The parameters correspond to our study where soil porosity (27 MAXSMC) and the hard-coded surface resistance parameter (59 KRSURF1) are the two most sensitive parameters for total runoff in almost all basins. But our study further demonstrates that total runoff is at least as sensitive to the Brooks-Corey parameter (26 BB), the slope of the stomatal conductance (23 MP), and vegetation height (10 HVT), as to saturated hydraulic conductivity (30 SATDK). Runoff is not only sensitive to soil parameters but it depends also strongly on water extraction by evapotranspiration and hence on vegetation. This is due to the water balance equation $\mathrm{d}S/\mathrm{d}t = P - E - Q$ with S water storage, P precipitation, E evapotranspiration (latent heat), and Q total runoff. Storage change $\mathrm{d}S/\mathrm{d}t$ is zero in steady state, and precipitation is hence partitioned between evapotranspiration E and runoff Q. If a parameter influences either E or Q, then it will inevitably influence the other. We observe, however, a general trend in the literature that hydrological studies focus on soil parameters within land surface models, while biogeoscience studies focus on vegetation parameters [e.g., *Santaren et al.*, 2014]. Sensitivity studies have, however, demonstrated that land surface models are sensitive to both soil and vegetation parameters not only for water but also for energy and carbon fluxes [*Prihodko et al.*, 2008; *Rosolem et al.*, 2012; *Göhler et al.*, 2013; *Lu et al.*, 2013], which is corroborated here.

We also found that latent heat has more interacting processes while the parameters seem to influence total runoff directly (Figures 3c and 3f). This can be exploited in parameter estimation since correlated parameters are a priori more difficult to constrain. Optimization procedures exist, however, that handle parameter correlations well, such as covariance matrix adaptation evolution strategies [*Hansen et al.*, 2003].

4.2. Hard-Coded Parameters

We have identified a multitude of hard-coded parameters within Noah-MP, of which a handful have sensitivities above 10% for the two observable outputs, latent heat and total runoff. The surface resistance parameter (59 KRSURF1) shows very high sensitivities. The formulation for Noah-MP comes from *Sakaguchi and Zeng* [2009] who replaced the original formulation of surface resistance of *Sellers et al.* [1992] in the land surface model CLM3.5 with a new formulation that includes vapor diffusion through the upper drying soil. KRSURF1 (59) determines how the thickness of the dry top layer increases with decreasing soil moisture. The formulation change had, however, little effect in the study of *Sakaguchi and Zeng* [2009] and our study demonstrates that it suffers possibly from an oversensitive parameter as well, just as in the original formulation [*Göhler et al.*, 2013]. *Sakaguchi and Zeng* [2009] suggested including a litter layer to dampen soil evaporation in closer accordance with previous evapotranspiration partitioning studies. A litter layer is, however, not as yet implemented in Noah-MP.

Latent heat and total runoff are also sensitive to the two input parameters that partition incoming solar radiation into direct and diffuse radiation (42 FDIRRAD) and into visible and near infrared (43 FVISRAD). The former

determines how deep incoming radiation can penetrate into the canopy; hence, how much of the radiation reaches the ground underneath the canopy, while the latter determines how much energy is available for assimilation. FDIRRAD (42) is taken as 70% in Noah-MP, independent of any atmospheric condition such as humidity or cloud coverage. FVISRAD (43) is taken as 50% but might well vary by 10–20% in nature [*Alados et al.*, 1996]. However, both parameters are only relevant if Noah-MP is not coupled to an atmospheric model such as WRF, which would provide different radiation bands (i.e., FVISRAD) as well as direct and diffuse radiation independently. The sensitivities of Noah-MP to the radiation input parameters indicate though that it would be sensible to give direct and diffuse radiation input directly to Noah-MP in off-line mode. Especially, studies calibrating Noah-MP locally against Eddy covariance data might want to feed this information directly to the model.

Sensitivities of snow parameters are much reduced for total runoff because of the ephemeral occurrence of surface runoff from snow and the relatively little surface runoff related to snow. Snow amount is always less than 20% of total precipitation even in the most snowy catchments (Table 2), and runoff associated with snow melt is therefore rather small. The large surface runoff fluxes are associated with summer rains rather than winter snow melt in Noah-MP. Snow melt leads to wetter soils, therefore enhanced drainage and hence subsurface runoff. The transfer of snow melt to runoff is therefore mediated by soil. Soil parameters show consequently large sensitivities (>1%) for total runoff, while snow parameters yield only very small sensitivity indexes. Any model calibration against streamflow data will hence not constrain the hard-coded snow parameters. Surface runoff, on the other hand, is sensitive (>1%) to almost all hard-coded snow parameters. The user has to treat the runoff time series in such a way that it accentuates the surface component if he wants to constrain the hard-coded snow parameters. This can be achieved by examining hydrological signatures such as rising limb density [*Shamir et al.*, 2005] or peak distribution [*Sawicz et al.*, 2011], which can be included in model calibration [*Shafii and Tolson*, 2015]. The hydrologic signatures can be more sensitive to snow parameters than the convoluted runoff signal and hence might allow better optimization of these less sensitive parameters. An alternative would be a Pareto optimization [e.g., *Asadzadeh and Tolson*, 2013] of discharge and snow height if the data are available for the catchment.

Hard-coded parameters of the radiation scheme (i.e., 56 C2STREAMCHIL1 and 57 C2STREAMCHIL4) show considerable sensitivities in evergreen forests (e.g., Amite River). These two parameters are in the Ross-Goudriaan function that approximates the projected leaf area depending on the leaf angle distribution function χ_L (5 XL) [e.g., *Sellers*, 1985]. This is an empirical function where *Goudriaan* [1977] fitted a function to data sets produced with *Ross*' [1975] χ_L function. The fitted parameters of the function have uncertainties, of course, and hence, they are not fixed physical constants.

4.3. Comparison With Earlier Studies With Noah-MP

Parameter sensitivities were already studied in parts for Noah-MP. *Cai et al.* [2014] examined the sensitivity of total runoff to three soil parameters (27 MAXSMC, 30 SATDK, and 59 KRSURF1), which included already the very sensitive hard-coded parameter of surface resistance (KRSURF1). They performed a qualitative sensitivity analysis by running Noah-MP with specific parameter values and visually comparing modeled total runoff. They found strong sensitivities for the three parameters chosen which is in line with our analysis. *Cai et al.* [2014] also pointed out that the surface resistance parameter (59 KRSURF1) can have strongly coupled effects also on latent heat, which we could confirm in all 12 MOPEX catchments. But as pointed out before, we found much more sensitive parameters than the three parameters chosen by *Cai et al.* [2014], both in the soil and also in the vegetation description of Noah-MP.

Mendoza et al. [2015] extracted another 11 hard-coded parameters from the model code, which included the following parameters (cf. Table A3): the minimum albedo of snow (50 CSNOWCLASSALB0), the decay constant for snow albedo with time (51 KSNOWCLASS), the albedo of fresh snow (52 CSNOWCLASSFRESH), the roughness length of snow surfaces (58 Z0SNO), the exponent in the dependence of snow melting on snow density (70 MEXP), the maximum liquid water holding capacity of snow (71 SNOW_IWC), and the snow water equivalent to fully cover the surface with snow (88 SWEMX). Another four parameters in runoff generation and groundwater extracted by *Mendoza et al.* [2015] are not active with our runoff option (Table A4).

Mendoza et al. [2015] calculated very different sensitivities compared to our Sobol' indexes. Their three most sensitive hard-coded parameters (50 CSNOCLASSALB0, 51 KSNOWCLASS, and 70 MEXP) are hardly noticeable in our case. *Mendoza et al.* [2015] used the Distributed Evaluation of Local Sensitivity Analysis (DELSA) [*Rakovec et al.*, 2014], which was designed to be a distributed version of the Sobol' analysis for the first-order

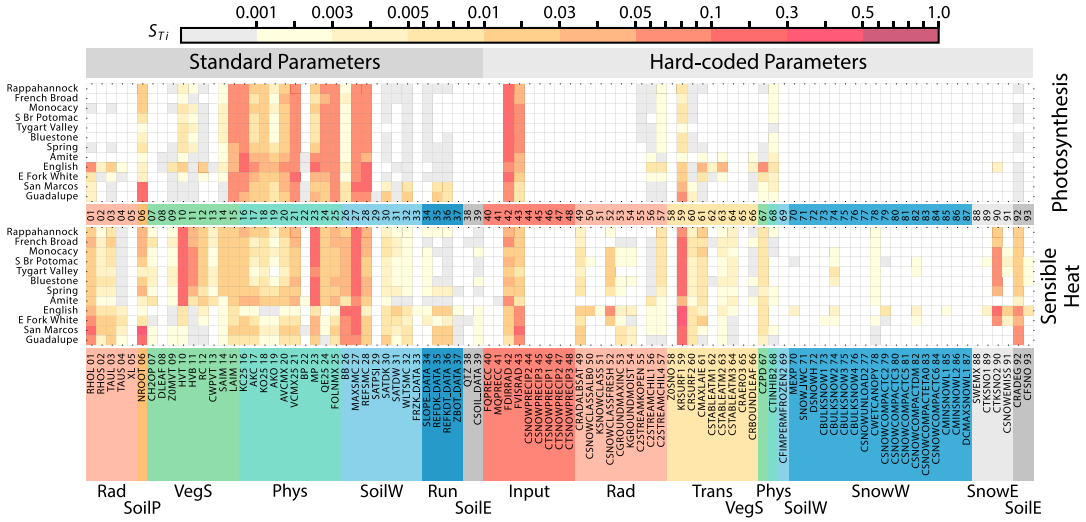

Figure 5. Same as Figure 4 but for photosynthesis and sensible heat. Sobol' indexes are variance-weighted averages in time.

Sobol' indexes, neglecting nonlinear model behavior and parameter interactions. Our results are overall quite similar between first and total-order Sobol' indexes for total runoff though (results not shown but compare Figure 3f for one basin). This implies that using DELSA's first-order approximation instead of total-order Sobol' indexes is not the reason for the large discrepancies in observed sensitivities. *Mendoza et al.* [2015] calculated sensitivity measures from modeling scores against observed discharge such as root-mean-square error (RMSE). This is susceptible to model bias, which means that indexes from RMSE and indexes from the mean bias are not independent, which could be resolved by using centered root-mean-square errors [*Taylor*, 2001]. *Cuntz et al.* [2015] argued that model sensitivities should be a model inherent property, independent of observations. Including observations in sensitivity measures convolutes changes in model output due to model parameter changes with apparent changes in model performance which come from compensation effects due to incomplete model formulations or data errors.

Probably, the largest source of discrepancy between this study and *Mendoza et al.* [2015] is that different parameter ranges have been used. *Mendoza et al.* [2015] considered parameter ranges found in the literature while we varied each parameter within 20% of its initial value. The decay constant of snow albedo (51 KSNOWCLASS) varied from 0.001 to 0.1, that means by 2 order of magnitudes in *Mendoza et al.* [2015], while it varied only from 0.08 to 0.12 in our case. Both DELSA and Sobol' indexes depend on the chosen parameter variations. This can easily be understood in DELSA where each local derivative is weighted by the corresponding parameter range. A parameter can, for example, have a small sensitivity index even if local sensitivities (derivatives) are large, but the parameter is considered well known, which means that it has a small parameter range. This explains most of the differences between *Mendoza et al.* [2015] and the study presented here. The choice of parameter ranges depends on the information required. A parameter might vary over several orders of magnitude between catchments such as saturated hydraulic conductivity (30 SATDK), but one might be able to constrain the parameter range within a given catchment a priori if, for example, one knows the soil composition. This would lead to much smaller parameter ranges and hence much smaller sensitivities. The former parameter sensitivities by varying parameters within their literature values might be interesting for model developers in order to examine if a process is important for all possible parameter values. Our parameter sensitivities using much smaller parameter ranges, on the other hand, might be needed by model users who aim to calibrate the model in a specific catchment with a minimum of model evaluations.

4.4. Sensitivities of Nonhydrologic Output Fluxes

We focus in this study on the hydrologic fluxes evapotranspiration and runoff, and their component fluxes. The Noah-MP land surface model calculates a closed energy balance and coupled water and carbon cycles. There are hence other variables that might be of interest for Noah-MP users. Figure 5 shows the same heatmaps as Figure 4 but for (gross) photosynthesis and sensible heat. The eddy covariance technique observes, however, net ecosystem exchange (NEE) next to latent and sensible heat. We did not calculate sensitivities of NEE

because this would have needed spinning up the soil carbon pools for several thousand years, a demanding undertaking for the 100,000 model runs computed in this study.

The total-order Sobol' indexes of photosynthesis look remarkably similar to the Sobol' indexes of transpiration, and the Sobol' indexes of sensible heat almost duplicate the indexes of latent heat (Figure 4). There are small differences though: the sensitivities of the photosynthesis parameters (category Phys) and of some radiation parameters (e.g., 42 FDIRRAD, 01 RHOL) are stronger for photosynthesis than for transpiration. This is compensated by less sensitivities of the vegetation structure parameters (category VegS) and of the soil resistance parameter KRSURF1 (59), the latter being still very sensitive for photosynthesis. Sensible heat exhibits mainly increased sensitivities to a number of radiation parameters. For example, the leaf optical properties (01 RHOL, 02 RHOS, 03 TAUL) show sensitivities above 1% and are not present in latent heat. But also, soil emissivity (92 CRADEG) and snow thermal conductivity (90 CTKSNO2) have larger sensitivities compared to latent heat.

We therefore deem it appropriate to focus on the hydrologic fluxes in this study because we included the component fluxes. Sensitivities of transpiration can be seen as a good approximation of the sensitivities of photosynthesis. Transpiration, on the other hand, helps in understanding the processes that lead to the sensitivities of latent heat as a combination of evaporation and transpiration.

It could have been expected that sensible and latent heat have (almost) equal sensitivities. Incoming energy is split into the two heat fluxes plus some storage in soil and canopy (e.g., soil heat flux). Storage is small compared to latent and sensible heat, which implies that the two fluxes vary inversely with parameter changes resulting in almost the same sensitivities.

4.5. Comparison With Sensitivities of Other Land Surface Models

Every land surface model implements different complexities for different processes. Sensitivities of one land surface model hence cannot be compared one to one, but the relative importance between processes should be similar in all land surface models. For example, all studies observe large sensitivities of latent and sensible heat to parameters in the stomatal conductance formulation such as the slope (23 MP) of the Ball-Woodrow-Berry formulation [*Ball et al.*, 1987]. This is true for Noah-MP and also for the Simple Biosphere (SiB) model in its revision 2.5 [*Prihodko et al.*, 2008] and in its revision 3.5 [*Rosolem et al.*, 2012, 2013], the Community Atmosphere Biosphere Land Exchange (CABLE) model [*Lu et al.*, 2013], the Common Land Model (CoLM) [*Li et al.*, 2013], the Lund-Potsdam-Jena General Ecosystem Simulator (LPJ-GUESS) [*Pappas et al.*, 2013], BIOME-BGC [*Raj et al.*, 2014], and the Community Land Model (CLM) revision 3.5 [*Göhler et al.*, 2013]. All the models exhibit also marked sensitivities for parameters in the photosynthesis submodule. This is directly carboxylation efficiency in Noah-MP (21 VCMX25), in SiB, in Cable, and in CoLM, whereas other parameters mostly relating $V_{C,\max}$ with nitrogen content are sensitive in LPJ-GUESS, BIOME-BGC, and CLM.

The picture starts fringing for soil parameters. Noah-MP, SiB, CoLM, and CLM are strongly sensitive to at least two of the three major soil parameters: porosity (27 MAXSMC), saturated hydraulic conductivity (30 SATDK), and the equivalents of the Brooks-Corey parameter (26 BB). LPJ-GUESS has sensitivity only to the maximum plant available water content, while CABLE is only sensitive to saturated hydraulic conductivity. All models manifest sensitivity to the availability of water to the plants, though, either through rooting depth (Noah-MP, CLM), the wilting point (CABLE, CoLM), or both (SiB, LPJ-GUESS). No soil or root variables were tested in the sensitivity analysis of BIOME-BGC [*Raj et al.*, 2014].

SiB and CABLE are structurally very similar to Noah-MP so that they are also sensitive (>1%) to canopy height. CLM should have the same sensitivity, but canopy height was no free parameter in the sensitivity analysis of CLM [*Göhler et al.*, 2013].

The magnitudes of the individual indexes in the above sensitivity analyses depend strongly on the chosen parameter ranges (except the analysis of CLM). A prominent example are the very different sensitivities of latent heat and photosynthesis in CABLE [*Lu et al.*, 2013]. Sensitivities of photosynthesis are completely dominated by the parameters $V_{C,\max}$ and leaf area index in CABLE, while latent heat shows much more distributed sensitivities, as outlined above. $V_{C,\max,25}$ was varied from 10 to 100 μmol m^{-2} s^{-1}, which is the whole range of possible $V_{C,\max,25}$ values for all PFTs in CABLE. The parameter range therefore encompasses very different vegetations such as savannah, boreal, and tropical forest. We opted for equal parameter ranges here, which reflects more the uncertainty of our parameter knowledge at a given place and which facilitates the comparison of sensitivities among parameters and fluxes. Latent heat and photosynthesis are therefore much closer linked in our study than, for example, in the sensitivity analysis of CABLE [*Lu et al.*, 2013].

5. Summary and Conclusions

We examined the computer source code of the Noah land surface model with multiple process options (Noah-MP) and identified 139 hard-coded numbers, which we termed hard-coded parameters. These parameters are thus fixed model constants in Noah-MP but bear uncertainty intrinsically because they result often from empirical or statistical descriptions of observed data at a given resolution and region. They carry also the same burden as the standard parameters of Noah-MP in that they have to represent the whole within-grid cell spatial heterogeneity in a single number. We therefore question whether the hard-coded parameters should be treated as constant values because of their influence on model output variability. A systematic global sensitivity analysis was thus performed for 42 active Noah-MP standard parameters, mostly given in tabulated form and distributed by given vegetation and soil input maps, as well as 75 active hard-coded parameters, which are mostly spatially constant. We considered the hydrologic output fluxes of Noah-MP in this study, in particular, the land surface-atmosphere exchange fluxes and the runoffs generated either at the soil surface or draining downward from the soil. Total runoff is thereby the sum of the latter two fluxes and would be input to a discharge generation and river runoff routing scheme, which would then produce temporal dynamics of streamflow.

Noah-MP is sensitive (>1%) to about two thirds of its applicable standard parameters, including parameters for vegetation structure, plant physiology, and soil water transport, while it is mostly insensitive to leaf optical properties. Noah-MP consistently shows a sensitivity to a number of hard-coded parameters, namely, one parameter of surface resistance (59 KRSURF1), two parameters partitioning incoming radiation into diffuse and direct radiation (42 FDIRRAD) and into visible and near-infrared radiation (43 FVISRAD), and one parameter for snow thermal conductivity (90 CTKSNO2). The following conclusions can be drawn:

1. Latent heat and total runoff show very similar sensitivities toward standard and hard-coded parameters. This would be expected because together they determine the long-term water balance. However, here it is because runoff is dominated by permanent subsurface runoff rather than ephemeral surface runoff and is hence dependent on available soil water, as is evapotranspiration.
2. Latent heat and total runoff are sensitive to both soil and plant parameters. This means that model calibrations of hydrologic or land surface models should take both soil and plant parameters into account and not only focus on one kind.
3. The formulation of evaporation seems to be oversensitive to a single parameter. An even stronger oversensitivity was observed in earlier formulations of evaporation and the issue was thus only slightly alleviated. The formulation should, therefore, be revisited or a litter layer should be introduced [*Sakaguchi and Zeng*, 2009; *Haverd and Cuntz*, 2010] to dampen the models sensitivity to the surface resistance parameter (59 KRSURF1).
4. Sensible and latent heat exhibit almost the same sensitivities so that calibration or sensitivity analysis can be performed with either of the two.
5. Photosynthesis has almost the same sensitivities as transpiration, which are different from the sensitivities of latent heat. Including photosynthesis and latent heat in model calibration might therefore be beneficial.
6. Noah-MP is sensitive to the quality of incoming radiation. The model user should therefore take care of the amount of direct to diffuse radiation and the amount of visible to near-infrared radiation in the input fields rather than letting Noah-MP crudely estimate these partitionings.
7. Radiation and its partitioning into canopy and soil available radiation is obviously important for land surface-atmosphere fluxes. The partitioning is dominated by structural features of the vegetation such as leaf area index and tree height, which should be accessible in spatially explicit form. But the partitioning depends also on the formulation of radiative transfer as it becomes apparent in watersheds dominated by evergreen coniferous forest (e.g., Amite River basin). New formulations combining structural and radiative transfer approaches might hence be required [*Haverd et al.*, 2012].
8. Surface runoff is sensitive to almost all hard-coded snow parameters. These sensitivities get diminished in total runoff. Hydrologic signatures might be a way to filter out the signal of surface runoff from a total runoff time series and hence access and constrain these hard-coded parameters.
9. A comparison with results of earlier studies highlights that parameter ranges have crucial influence on sensitivities. These must be chosen wisely for the application of interest.

Only the few most sensitive parameters identified in this study, e.g., all parameters with sensitivities greater than 1% for a specific output flux, might be considered in future studies that focus, for example, on calibrating Noah-MP for improving the reliability of simulated hydrologic fluxes, or on developing multiscale parameter

regionalizations [*Samaniego et al.*, 2010]. Some of the most sensitive parameters were, however, hard-coded in the model code and have been made available to users of Noah-MP through this study.

Appendix A: Standard and Hard-Coded Parameters of Noah-MP

Table A1 gives the standard parameters of Noah-MP that are used in the model code and are active with the chosen process options and output fluxes of evapotranspiration (latent heat) and runoff. Parameters in Table A2 are the standard parameters used in the model code but active only with other process options such as using a groundwater storage or other output fluxes such as respiration. Tables A3 and A4 list all so-called hard-coded parameters that were found in the code. The tables are split again into parameters that are active with the chosen process options and output fluxes (Table A3) and into parameters that belong to process options and output fluxes that are not considered in this study (Table A4).

Table A1. Active Standard Parameters of Noah-MP With the Chosen Process Options and Output Fluxes[a]

#	Code	Category	Description
MPTable.tbl			
1	RHOL	Rad	Leaf reflectivity
2	RHOS	Rad	Stem reflectivity
3	TAUL	Rad	Leaf transmissivity
4	TAUS	Rad	Stem transmissivity
5	XL	Rad	Leaf angle distribution parameter
7	CH2OP	VegS	Maximum intercepted water per leaf and stem area
8	DLEAF	VegS	Leaf characteristic length for leaf boundary layer conductance
9	Z0MVT	VegS	Roughness length (for momentum)
10	HVT	VegS	Vegetation height
11	HVB	VegS	Height of lower canopy bound
12	RC	VegS	Horizontal crown radius
13	CWPVT	VegS	Extinction parameter for wind in canopy
14	SAIM	VegS	Monthly maximum stem area index
15	LAIM	VegS	Monthly maximum leaf area index
16	KC25	Phys	Michaelis-Menten constant for carboxylation of RuBisCO
17	AKC	Phys	Q_{10} temperature dependence of carboxylation of RuBisCO
18	KO25	Phys	Michaelis-Menten constant for oxygenation of RuBisCO
19	AKO	Phys	Q_{10} temperature dependence of oxygenation of RuBisCO
20	AVCMX	Phys	Q_{10} temperature dependence of $V_{C,max}$
21	VCMX25	Phys	Maximum carboxylation rate $V_{C,max}$ at 25°C
22	BP	Phys	Intercept of Ball-Woodrow-Berry stomatal conductance formulation [*Ball et al.*, 1987]
23	MP	Phys	Slope of Ball-Woodrow-Berry stomatal conductance formulation [*Ball et al.*, 1987]
24	QE25	Phys	Maximum electron transport rate J_{max} at 25°C
25	FOLNMX	Phys	Foliage nitrogen concentration before limitation
	C3PSN[b]	Phys	True for C_3 photosynthetic pathway
	TMIN	C	Minimum growth temperature
	WDPOOL[b]	C	True for woody vegetation
VegParm.tbl			
6	NROOT	SoilP	Number of soil layers with roots
SoilParm.tbl			
26	BB	SoilW	Exponent in Brooks-Corey relation between volumetric soil moisture and soil matric potential
27	MAXSMC	SoilW	Soil porosity
28	REFSMC	SoilW	Volumetric soil water content at field capacity
29	SATPSI	SoilW	Soil matric potential at saturation

Table A1. (continued)

#	Code	Category	Description
30	SATDK	SoilW	Soil hydraulic conductivity at saturation
31	SATDW	SoilW	Soil water diffusivity at saturation
32	WLTSMC	SoilW	Volumetric soil water content at wilting point
38	QTZ	SoilE	Relative quartz content of soil
GenParm.tbl			
33	FRZK_DATA	SoilW	Ice content above which soil is impermeable
34	SLOPE_DATA	Run	Factor on hydraulic conductivity for soil drainage
35	REFDK_DATA	Run	Hydraulic conductivity at saturation for silt clay loamy soil
36	REFKDT_DATA	Run	Related to surface infiltration factor
37	ZBOT_DATA	Run	Soil depth for soil temperature calculations
39	CSOIL_DATA	SoilE	Volumetric heat capacity of soil particles

[a]The symbol "#" is the number on the abscissae of Figures 3 and 4. There is no number assigned to noninformative parameters for any output flux with the chosen process options. "Code" is the name in the Fortran code and in the header lines of the tabulated input files MPTable.tbl, VegParm.tbl, SoilParm.tbl, GenParm.tbl. "Category" arranges the variables in groups for representation in the text. Abbreviations in the categories, the following tables and the figures are —C: Carbon; Input: Input; Phys: Physiology; Rad: Radiation; Run: Runoff; SnowE: Snow energy; SnowW: Snow water; SoilE: Soil energy; SoilP: Soil-Physiology interactions; SoilW: Soil water; Trans: Transfer; VegS: Vegetation structure; VOC: Volatile organic carbon.

[b]Both C3PSN and WDPOOL are active variables but are rather characteristics than parameters and therefore not changed during the sensitivity analysis.

Table A2. Inactive Standard Parameters of Noah-MP With the Chosen Process Options and Output Fluxes[a]

Code	Category	Description
MPTable.tbl		
AQE	Phys	Q_{10} temperature dependence of J_{max}
ARM	C	Q_{10} temperature dependence of leaf respiration
EPS	VOC	Volatile organic carbon (VOC) emission factor
DILEFC	C	Base rate factor for leaf fall with temperature
DILEFW	C	Base rate factor for leaf fall with soil moisture
FRAGR	C	Fraction of net assimilation for growth respiration
LTOVRC	C	Leaf turnover rate
MRP	C	Factor for microbial influence on soil respiration
RMF25	C	Leaf respiration rate at 25°C
RMR25	C	Root respiration at 25°C
RMS25	C	Stem respiration at 25°C
SLA	C	Specific leaf area for carbon fluxes
SLAREA	VOC	Specific leaf area for volatile organic carbon (VOC) fluxes
TDLEF	Phys	Characteristic temperature for leaf freezing
WRRAT	C	Ratio woody to nonwoody parts of plants
VegParm.tbl		
HS	Phys	Sensitivity of stomata to vapor pressure deficit in *Jarvis* [1976] formulation
RGL	Phys	Slope of stomatal response to radiation in *Jarvis* [1976] formulation
RS	Phys	Minimum stomatal resistance in *Jarvis* [1976] formulation
RSMAX_DATA	Phys	Maximum stomatal resistance in *Jarvis* [1976] formulation
SHDFAC	VegS	Fraction of vegetated area per grid cell
TOPT_DATA	Phys	Optimal temperature for photosynthesis
GenParm.tbl		
CZIL_DATA	Trans	Zilitinkevich factor, ratio of roughness lengths of heat to momentum

[a]Table columns are as in Table A1 but without the number for the plots, which is irrelevant for inactive parameters.

Table A3. Active Hard-Coded Parameters With the Chosen Process Options and Output Fluxes[a]

#	Code (Value)	Category	Description
40	FQPRECC (0.1)	Input	Fraction of convective precipitation on total precipitation
41	MQPRECC (10.0)	Input	Multiplier to convective precipitation for fractional area that receives precipitation
42	FDIRRAD (0.7)	Input	Fraction of direct vs. diffuse shortwave radiation
43	FVISRAD (0.5)	Input	Fraction of visible vs. near infrared shortwave radiation
44	CSNOWPRECIP2 (0.2)	Input	In partitioning of total precipitation into liquid precipitation water and snow
45	CSNOWPRECIP3 (0.6)	Input	In partitioning of total precipitation into liquid precipitation water and snow
46	CTSNOWPRECIP1 (0.5)	Input	In temperature thresholds for partitioning of total precipitation into liquid precipitation water and snow
47	CTSNOWPRECIP2 (1.5)	Input	In temperature thresholds for partitioning of total precipitation into liquid precipitation water and snow
48	CTSNOWPRECIP3 (0.5)	Input	In temperature thresholds for partitioning of total precipitation into liquid precipitation water and snow
49	CRADALBSAT[b]	Rad	Multiplier to albedos of saturated soils
50	CSNOWCLASSALB0 (0.55)	Rad	Minimum albedo of snow
51	KSNOWCLASS (0.01)	Rad	Decay constant of snow albedo with time
52	CSNOWCLASSFRESH (0.84)	Rad	Albedo of fresh snow
53	CGROUNDMAXINC (0.11)	Rad	Maximum increment of albedo of dry soils compared to wet soils
54	KGROUNDMOIST (0.4)	Rad	Change of ground albedo with moisture
55	C2STREAMKOPEN (0.05)	Rad	Between-crown gap probability for diffuse radiation
56	C2STREAMCHIL1 (0.5)	Rad	In Ross-Goudriaan function that approximates the projected leaf area depending on leaf angle distribution
57	C2STREAMCHIL4 (0.877)	Rad	In Ross-Goudriaan function that approximates the projected leaf area depending on leaf angle distribution
58	Z0SNO (0.002)	Trans	Roughness length of snow surfaces
59	KRSURF1 (5.0)	Trans	Controlling concavity of the soil dry layer thickness with saturation
60	CRSURF2 ($2.2 \cdot 10^{-5}$)	Trans	Molecular diffusion coefficient of water vapor
61	CMAXLAIE (6.0)	Trans	Maximum effective LAI in vegetation clump
62	CSTABLEATM1 (16.0)	Trans	In atmospheric stability function in boundary layer (unstable conditions)
63	CSTABLEATM2 (0.25)	Trans	In atmospheric stability function in boundary layer (unstable conditions)
64	CSTABLEATM3 (5.0)	Trans	In atmospheric stability function in boundary layer (stable conditions)
65	CRAERO3 (4.7)	Trans	In atmospheric stability function for aerodynamic resistance (stable conditions)
66	CRBOUNDLEAF (50.0)	Trans	In leaf boundary layer resistance
67	CZPD (0.65)	VegS	Ratio of displacement height to vegetation height
68	CTINHIB2 (710.0)	Phys	Temperature inhibition of enzymatic reactions
69	CFIMPERMFROZEN2 (3.0)	SoilW	Impermeable fraction due to frozen soil
70	MEXP (1.0)	SnowW	Exponent in dependence of snow melting on snow density
71	SNOW_IWC (0.03)	SnowW	Maximum liquid water capacity of snow
72	DSNOWH (0.2)	SnowW	Decay constant for snow cover fraction of short vegetation with snow height
73	CBULKSNOW1 (120.0)	SnowW	Minimum bulk density of fresh snow
74	CBULKSNOW2 (67.92)	SnowW	In bulk density of fresh snow dependence on temperature
75	CBULKSNOW3 (51.25)	SnowW	In bulk density of fresh snow dependence on temperature
76	CBULKSNOW4 (2.59)	SnowW	In bulk density of fresh snow dependence on temperature
77	CSNOWUNLOAD2 ($1.56 \cdot 10^{5}$)	SnowW	Wind unloading factor of snow on canopy
78	CWETCANOPY (0.667)	SnowW	Wet canopy fraction
79	CSNOWCOMPACTC2 (0.021)	SnowW	In snow compaction scheme
80	CSNOWCOMPACTC3 ($2.5 \cdot 10^{-6}$)	SnowW	In snow compaction scheme
81	CSNOWCOMPACTC5 (2.0)	SnowW	In snow compaction scheme

Table A3. (continued)

#	Code (Value)	Category	Description
82	CSNOWCOMPACTDM (100.0)	SnowW	In snow compaction scheme
83	CSNOWCOMPACTETA0 (8.0^5)	SnowW	In snow compaction scheme
84	CSNOWCOMPACTC6 (0.046)	SnowW	In snow compaction scheme
85	CMINSNOWL1 (0.025)	SnowW	Minimum height of first snow layer
86	CMINSNOWL2 (0.025)	SnowW	Minimum height of second snow layer
87	DCMAXSNOWL1 (0.0)	SnowW	To minimum height of first snow layer
88	SWEMX (1.0)	SnowE	Amount of fresh snow (water equivalent) for fully covering old snow
89	CTKSNO1 ($3.2217 \cdot 10^{-6}$)	SnowE	Thermal conductivity of very fluffy snow
90	CTKSNO2 (2.0)	SnowE	Exponential dependence of thermal conductivity on snow density
91	CSNOWEMISS (1.0)	SnowE	Snow emissivity
92	CRADEG[b]	SoilE	Ground emissivities of soils and lakes
93	CFSNO (2.5)	SoilE	In snowy grid cell fraction
	ALBDRY[b]	Rad	Dry soil albedos
	BETADS[b] (0.5)	Rad	Upscatter parameter of snow for diffuse radiation
	BETAIS[b] (0.5)	Rad	Upscatter parameter of snow for direct beam radiation
	CCIC3 (0.7)	Phys	Stomatal to atmospheric CO_2 concentration ratio for nonwater limited C_3 plants
	CDFFRESH (0.35)	SnowE	Thermal conductivity of fresh snow
	CFIMPERMFROZEN1 (4.0)	SoilW	In impermeable fraction due to frozen soil
	CMAXSNO1 (6.6)	SnowW	In maximum snow amount of canopy
	CMAXSNO2 (0.27)	SnowW	In maximum snow amount of canopy
	CMAXSNO3 (46)	SnowW	In maximum snow amount of canopy
	CMINSNOWL3 (0.1)	SnowW	Minimum height of third snow layer
	CRAERO1 (15.0)	Trans	In atmospheric stability function for aerodynamic resistance (unstable conditions)
	CRAERO2 (0.25)	Trans	In atmospheric stability function for aerodynamic resistance (unstable conditions)
	CSNOWCOMPACTC4 (0.04)	SnowW	In snow compaction scheme
	CSNOWCOMPACTC7 (0.08)	SnowW	In snow compaction scheme
	CSNOWUNLOAD1 ($1.87 \cdot 10^5$)	SnowW	Temperature unloading factor of snow on canopy
	CSTABLEATM4 (0.9)	Trans	In atmospheric stability function in boundary layer
	CTHKDRY1 (0.135)	SoilE	In dependence of thermal conductivity of dry soil on bulk density
	CTHKDRY2 (64.7)	SoilE	In dependence of thermal conductivity of dry soil on bulk density
	CTHKDRY3 (0.947)	SoilE	In dependence of thermal conductivity of dry soil on bulk density
	DMAXSNOWL2 (0.2)	SnowW	Maximum height of second snow layer
	OMEGAS[b]	Rad	Scattering albedos of snow

[a]Table columns as in Table A1.
[b]Radiation parameters for visible and near infrared of the different soils are given as hard-coded data in the model code, instead of the usual form in tabulated files (cf. Tables A1 and A2).

Table A4. Inactive hard-coded parameters with the chosen process options and output fluxes[a]

Code	Category	Description
CBASEFLOWMAX1 (4.0)	Run	Baseflow coefficient for runoff option 2
CBASEFLOWMAX2 (5.0)	Run	Baseflow coefficient for runoff option 1
CBELJAARS1 (1.2)	Trans	In Beljaar's correction for convective wind for surface layer option 2
CBELJAARS2 (270.0)	Trans	In Beljaar's correction for convective wind for surface layer option 2
CBELJAARS3 (1000.0)	Trans	In Beljaar's correction for convective wind for surface layer option 2

Table A4. (continued)

Code	Category	Description
CBF (0.9)	C	Allocation of new carbon to roots
CCIC4 (0.4)	Phys	Stomatal to atmospheric CO_2 concentration ratio for nonwater limited C_4 plants
CCMIC (0.2)	Run	Micropore water content for groundwater for runoff option 1
CDIELEAF1 (0.3)	C	In seasonal leaf die rate dependence on temperature
CDIELEAF2 (120.0)	C	In seasonal leaf die rate dependence on temperature
CDFURB (3.24)	SoilE	Thermal conductivity of urban land cover
CFCARBLEAF (0.75)	C	Fraction of new carbon allocation into leaves
CFCARBSTEM (10.0)	C	Fraction of new carbon allocation into stems
CFFFRUNOFF1 (2.0)	Run	Saturated area decay factor for runoff option 1
CFFFRUNOFF2 (6.0)	Run	Runoff decay factor for runoff option 1
CFFFRUNOFF3 (6.0)	Run	Runoff decay factor for runoff option 5
CFFFRUNOFF4 (2.0)	Run	Saturated area decay factor for runoff option 2
CFFFRUNOFF5 (6.0)	Run	Runoff decay factor for runoff option 2
CFSATEXP (4.0)	Run	Exponent for fraction of saturated area in runoff option 4
CFSTABLRSOIL (0.1)	C	Fraction of soil respiration going to stable carbon
CFURBAN (0.95)	Run	Fraction of sealed area at urban land class
CFWRSOIL1 (0.2)	C	In water limitation of soil respiration
CFWRSOIL2 (0.23)	C	In water limitation of soil respiration
CGROUNDANG1 (1.7)	Rad	In albedo for diffuse radiation of lakes
CGROUNDANG2 (0.15)	Rad	In albedo for diffuse radiation of lakes
CGROUNDDESERT (0.1)	Rad	Increment of soil albedo in deserts
CGROUNDEMISS (0.98)	SoilE	Emissivity of frozen ground
CGROUNDLAKEI (0.06)	Rad	In albedo for diffuse radiation of lakes
CINITWTD (3.0)	Run	Initial equilibrium water table depth for runoff option 2
CKOREN (8.0)	SoilW	In supercooled liquid water option 2
CLECH1 (0.96)	Trans	In Lech's stability functions for surface layer option 2
CLECH2 (4.5)	Trans	In Lech's stability functions for surface layer option 2
CLECH3 (2.076)	Trans	In Lech's stability functions for surface layer option 2
CMAXGLACIERH (2000.0)	SnowW	Maximum snow water depth
CMAXGROUND (5000.0)	Run	Maximum groundwater storage for runoff option 2
CMINWTD (1.5)	Run	Minimum groundwater table depth for runoff option 2
CPAULSON (5.0)	Trans	In Paulson's stability function for surface layer option 2
CQ10 (0.08)	C	Q_{10} of wood respiration
CQ10RSOIL (2.0)	C	Q_{10} for soil respiration
CRADALBICE (1.0)	Rad	For albedo of land ice
CRADALBLAK (1.0)	Rad	For albedo of frozen lakes
CRSWOODC (3.0^{-10})	C	Coefficient for wood respiration
CRF (0.5)	C	Reduction factor for respiration in nongrowing season
CROUS (0.2)	Run	Specific groundwater yield for runoff option 2
CRTOVRC (2.0^{-8})	C	Root turnover rate per time step
CSNOWAGE1 (5000.0)	SnowE	In snow ageing
CSNOWAGE2 (10.0)	SnowE	In snow ageing
CSNOWAGE3 (0.3)	SnowE	In snow ageing
CSNOWBATSC1 (0.2)	SnowE	In snow ageing for snow albedo scheme 1
CSNOWBATSC2 (0.5)	SnowE	In snow ageing for snow albedo scheme 1
CSNOWBATSNIR (0.65)	Rad	Albedo of fresh snow in the near infrared for snow albedo scheme 1
CSNOWBATSVIS (0.95)	Rad	Albedo of fresh snow in the visible for snow albedo scheme 1

Table A4. (continued)

Code	Category	Description
CSNOWBATSSL (2.0)	SnowE	In zenith angle correction for snow albedo scheme 1
CTSNOWPRECIP4 (2.2)	Input	In temperature thresholds for partitioning of total precipitation into liquid precipitation water and snow in partitioning option 2
CWDFICE1 (500.0)	SoilW	In water diffusivity when ice present for frozen soil permeability option 2
CWDFICE2 (3.0)	SoilW	In water diffusivity when ice present for frozen soil permeability option 2
CWDFICE3 (0.2)	SoilW	In water diffusivity when ice present for frozen soil permeability option 2
CWOODTOV ($9.5 \cdot 10^{-10}$)	C	Wood turn over rate per time step
CWSTRC (100.0)	C	In water stress function for leaf die off
DFCARBLEAFEBL (0.5)	C	In fraction of new carbon into leaves for evergreen broadleaf forests
FSATMX (0.38)	Run	Sum of fractional lowland areas for runoff option 1
KFVEG (0.52)	VegS	Canopy light extinction coefficient for dynamic vegetation options 2 and 3
KSSIBPSI (5.8)	SoilP	Exponential decay of stomatal resistance with soil moisture for soil moisture limitation option 3
TIMEAN (10.5)	SoilW	Grid cell mean topographic index for runoff options 1 and 2

[a]Table columns are as in Table A1 but without the number for the plots, which is irrelevant for inactive parameters.

Acknowledgments
We would like to thank Aubrey Dugger and David Gochis (NCAR) for providing information of runoff sensitivities on Noah-MP options. We thank Michael Barlage (NCAR) for general insights into Noah-MP. All participants of the North American Land Data Assimilation System project (NLDAS) are acknowledged. The NLDAS project is a collaboration project jointly between NCEP, NASA Goddard Space Flight Center, Princeton University, and University of Washington sponsored by NOAA's Climate Program Office and NASA's Terrestrial Hydrology Program. We thank Rafael Rosolem and two anonymous reviewers for their careful comments that greatly improved the final manuscript. The study is a contribution to the Helmholtz-Association climate initiative REKLIM.

References

Alados, I., I. Foyo-Moreno, and L. Alados-Arboledas (1996), Photosynthetically active radiation: Measurements and modelling, *Agric. For. Meteorol.*, *78*, 121–131.

Asadzadeh, M., and B. Tolson (2013), Pareto archived dynamically dimensioned search with hypervolume-based selection for multi-objective optimization, *Eng. Optim.*, *45*, 1489–1509.

Ball, J. T., I. E. Woodrow, and J. A. Berry (1987), A model predicting stomatal conductance and its contribution to the control of photosynthesis under different environmental conditions, in *Progress in Photosynthesis Research*, edited by J. Biggens, pp. 221–224, Springer, Netherlands.

Barlage, M., M. Tewari, F. Chen, G. Miguez-Macho, Z.-L. Yang, and G.-Y. Niu (2015), The effect of groundwater interaction in North American regional climate simulations with WRF/Noah-MP, *Clim. Change*, *129*, 485–498.

Best, M. J., et al. (2015), The plumbing of land surface models: Benchmarking model performance, *J. Hydrometeorol.*, *16*, 1425–1442.

Bierkens, M. F. P., et al. (2015), Hyper-resolution global hydrological modelling: What is next?, *Hydrol. Processes*, *29*, 310–320.

Brooks, R. H., and A. T. Corey (1964), Hydraulic properties of porous media, *Tech. Rep. 3*, Colorado State Univ., Fort Collins, Colo.

Brutsaert, W. (1982), *Evaporation Into the Atmosphere, Theory, History and Applications*, Springer, Dordrecht, Netherlands.

Cai, X., Z.-L. Yang, C. H. David, G.-Y. Niu, and M. Rodell (2014), Hydrological evaluation of the Noah-MP land surface model for the Mississippi River Basin, *J. Geophys. Res. Atmos.*, *119*, 23–38, doi:10.1002/2013JD020792.

Chen, F., and J. Dudhia (2001), Coupling an advanced land surface-hydrology model with the Penn State-NCAR MM5 modeling system. Part I: Model implementation and sensitivity, *Mon. Weather Rev.*, *129*(4), 569–585.

Chen, F., K. Mitchell, J. Schaake, Y. K. Xue, H. L. Pan, V. Koren, Q. Y. Duan, M. Ek, and A. Betts (1996), Modeling of land surface evaporation by four schemes and comparison with FIFE observations, *J. Geophys. Res.*, *101*(D3), 7251–7268.

Clark, M. P., et al. (2015a), A unified approach for process-based hydrologic modeling: 1. Modeling concept, *Water Resour. Res.*, *51*, 2498–2514, doi:10.1002/2015WR017198.

Clark, M. P., et al. (2015b), A unified approach for process-based hydrologic modeling: 2. Model implementation and case studies, *Water Resour. Res.*, *51*, 2515–2542, doi:10.1002/2015WR017200.

Claussen, M., K. Selent, V. Brovkin, T. Raddatz, and V. Gayler (2013), Impact of CO_2 and climate on Last Glacial Maximum vegetation—A factor separation, *Biogeosciences*, *10*, 3593–3604.

Cuntz, M., et al. (2015), Computationally inexpensive identification of noninformative model parameters by sequential screening, *Water Resour. Res.*, *51*, 6417–6441, doi:10.1002/2015WR016907.

Demaria, E. M., B. Nijssen, and T. Wagener (2007), Monte Carlo sensitivity analysis of land surface parameters using the Variable Infiltration Capacity model, *J. Geophys. Res.*, *112*, D11113, doi:10.1029/2006JD007534.

Duan, Q., et al. (2006), Model Parameter Estimation Experiment (MOPEX): An overview of science strategy and major results from the second and third workshops, *J. Hydrol.*, *320*, 3–17.

Ek, M. B., K. E. Mitchell, Y. Lin, E. Rogers, P. Grunmann, V. Koren, G. Gayno, and J. D. Tarpley (2003), Implementation of Noah land surface model advances in the National Centers for Environmental Prediction operational mesoscale Eta model, *J. Geophys. Res.*, *108*(D22), 8851, doi:10.1029/2002JD003296.

Fisher, J. B., D. N. Huntzinger, C. R. Schwalm, and S. Sitch (2014), Modeling the terrestrial biosphere, *Annu. Rev. Environ. Resour.*, *39*, 91–123.

Friedl, M. A., J. Hodges, and A. H. Strahler (2010), ISLSCP II MODIS (collection 4) IGBP land cover, 2000–2001, in *ISLSCP Initiative II Collection*, edited by F. G. Hall et al., Oak Ridge Natl. Lab. Distrib. Active Arch. Cent., Oak Ridge, Tenn.

Gochis, D., W. Yu, and D. Yates (2013), The WRF-Hydro Model Technical Description and User's Guide, Version 1.0, NCAR Technical Document, 120 pp., NCAR, Boulder, Colo. [Available at http://www.ral.ucar.edu/projects/wrf_hydro/.]
Göhler, M., J. Mai, and M. Cuntz (2013), Use of eigendecomposition in a parameter sensitivity analysis of the Community Land Model, *J. Geophys. Res. Biogeosci.*, *118*, 904–921, doi:10.1002/jgrg.20072.
Goudriaan, J. (1977), Crop micrometeorology: A simulation study, PhD thesis, Simulation Monographs, Pudoc, Wageningen, Netherlands.
Hansen, N., S. D. Müller, and P. Koumoutsakos (2003), Reducing the time complexity of the derandomized evolution strategy with covariance matrix adaptation (CMA-ES), *Evol. Comput.*, *11*(1), 1–18.
Haverd, V., and M. Cuntz (2010), Soil-Litter-Iso: A one-dimensional model for coupled transport of heat, water and stable isotopes in soil with a litter layer and root extraction, *J. Hydrol.*, *388*, 438–455.
Haverd, V., J. L. Lovell, M. Cuntz, D. L. B. Jupp, G. J. Newnham, and W. Sea (2012), The Canopy Semi-analytic P_{gap} and Radiative Transfer (CanSPART) model: Formulation and application, *Agric. For. Meteorol.*, *160*, 14–35.
Jarvis, P. G. (1976), The interpretation of the variations in leaf water potential and stomatal conductance found in canopies in the field, *Philos. Trans. R. Soc. B*, *273*, 593–610.
Jordan, R. (1991), A one-dimensional temperature model for a snow cover, *Tech. Rep. Spec. Rep. 91-16*, US Army Corps of Eng., Cold Regions Res. and Eng. Lab., Hanover, N. H.
Li, J., Q. Y. Duan, W. Gong, A. Ye, Y. Dai, C. Miao, Z. Di, C. Tong, and Y. Sun (2013), Assessing parameter importance of the Common Land Model based on qualitative and quantitative sensitivity analysis, *Hydrol. Earth Syst. Sci.*, *17*, 3279–3293.
Lu, X., Y.-P. Wang, T. Ziehn, and Y. Dai (2013), An efficient method for global parameter sensitivity analysis and its applications to the Australian community land surface model (CABLE), *Agric. For. Meteorol.*, *182–183*, 292–303.
Mendoza, P. A., M. P. Clark, M. Barlage, B. Rajagopalan, L. Samaniego, G. Abramowitz, and H. Gupta (2015), Are we unnecessarily constraining the agility of complex process-based models?, *Water Resour. Res.*, *51*, 716–728, doi:10.1002/2014WR015820.
Miller, D. A., and R. A. White (1998), A conterminous United States multilayer soil characteristics dataset for regional climate and hydrology modeling, *Earth Interact.*, *2*(2), 25.
Milly, P. C. D., S. L. Malyshev, E. Shevliakova, K. A. Dunne, K. L. Findell, T. Gleeson, Z. Liang, P. Phillipps, R. J. Stouffer, and S. Swenson (2014), An enhanced model of land water and energy for global hydrologic and Earth-system studies, *J. Hydrometeorol.*, *15*, 1739–1761.
Morris, M. D. (1991), Factorial sampling plans for preliminary computational experiments, *Technometrics*, *33*(2), 161–174.
Niu, G.-Y., and Z.-L. Yang (2006), Effects of frozen soil on snowmelt runoff and soil water storage at a continental scale, *J. Hydrometeorol.*, *7*(5), 937–952.
Niu, G.-Y., et al. (2011), The community Noah land surface model with multiparameterization options (Noah-MP): 1. Model description and evaluation with local-scale measurements, *J. Geophys. Res.*, *116*, D12109, doi:10.1029/2010JD015139.
Pappas, C., S. Fatichi, S. Leuzinger, A. Wolf, and P. Burlando (2013), Sensitivity analysis of a process-based ecosystem model: Pinpointing parameterization and structural issues, *J. Geophys. Res. Biogeosci.*, *118*, 505–528, doi:10.1002/jgrg.20035.
Peters-Lidard, C. D., E. Blackburn, X. Liang, and E. F. Wood (1998), The effect of soil thermal conductivity parameterization on surface energy fluxes and temperatures, *J. Atmos. Sci.*, *55*(7), 1209–1224.
Prentice, I. C., W. Cramer, S. P. Harrison, R. Leemans, R. A. Monserud, and A. M. Solomon (1992), A global biome model based on plant physiology and dominance, soil properties and climate, *J. Biogeogr.*, *19*, 117–134.
Prihodko, L., A. S. Denning, N. P. Hanan, I. Baker, and K. Davis (2008), Sensitivity, uncertainty and time dependence of parameters in a complex land surface model, *Agric. For. Meteorol.*, *148*(2), 268–287.
Raj, R., N. A. S. Hamm, C. van der Tol, and A. Stein (2014), Variance-based sensitivity analysis of BIOME-BGC for gross and net primary production, *Ecol. Modell.*, *292*, 26–36.
Rakovec, O., M. C. Hill, M. P. Clark, A. H. Weerts, A. J. Teuling, and R. Uijlenhoet (2014), Distributed Evaluation of Local Sensitivity Analysis (DELSA), with application to hydrologic models, *Water Resour. Res.*, *50*, 409–426, doi:10.1002/2013WR014063.
Rayner, P. J., M. Scholze, W. Knorr, T. Kaminski, R. Giering, and H. Widmann (2005), Two decades of terrestrial carbon fluxes from a Carbon Cycle Data Assimilation System (CCDAS), *Global Biogeochem. Cycles*, *19*, GB2026, doi:10.1029/2004GB002254.
Rosero, E., Z.-L. Yang, T. Wagener, L. E. Gulden, S. Yatheendradas, and G.-Y. Niu (2010), Quantifying parameter sensitivity, interaction, and transferability in hydrologically enhanced versions of the Noah land surface model over transition zones during the warm season, *J. Geophys. Res.*, *115*, D03106, doi:10.1029/2009JD012035.
Rosolem, R., H. V. Gupta, W. J. Shuttleworth, X. Zeng, and L. G. G. de Gonçalves (2012), A fully multiple-criteria implementation of the Sobol' method for parameter sensitivity analysis, *J. Geophys. Res.*, *117*, D07103, doi:10.1029/2011JD016355.
Rosolem, R., H. V. Gupta, W. J. Shuttleworth, L. G. G. de Gonçalves, and X. Zeng (2013), Towards a comprehensive approach to parameter estimation in land surface parameterization schemes, *Hydrol. Processes*, *27*(14), 2075–2097.
Ross, J. (1975), Radiative transfer in plant communities, in *Vegetation and the Atmosphere*, vol. 1, edited by J. L. Monteith, pp. 13–52, Academic Press, London.
Running, S. W., and J. C. Coughlan (1988), A general-model of forest ecosystem processes for regional applications—1. Hydrologic balance, canopy gas-exchange and primary production processes, *Ecol. Modell.*, *42*(2), 125–154.
Sakaguchi, K., and X. Zeng (2009), Effects of soil wetness, plant litter, and under-canopy atmospheric stability on ground evaporation in the Community Land Model (CLM3.5), *J. Geophys. Res.*, *114*, D01107, doi:10.1029/2008JD010834.
Saltelli, A., M. Ratto, T. H. Andres, F. Campolongo, J. Cariboni, D. Gatelli, M. Saisana, and S. Tarantola (2008), *Global Sensitivity Analysis. The Primer*, John Wiley, Chichester, U. K.
Samaniego, L., R. Kumar, and S. Attinger (2010), Multiscale parameter regionalization of a grid-based hydrologic model at the mesoscale, *Water Resour. Res.*, *46*, W05523, doi:10.1029/2008WR007327.
Santaren, D., P. Peylin, N. Viovy, and P. Ciais (2007), Optimizing a process-based ecosystem model with eddy-covariance flux measurements: A pine forest in southern France, *Global Biogeochem. Cycles*, *21*, GB2013, doi:10.1029/2006GB002834.
Santaren, D., P. Peylin, C. Bacour, P. Ciais, and B. Longdoz (2014), Ecosystem model optimization using in situ flux observations: Benefit of Monte Carlo versus variational schemes and analyses of the year-to-year model performances, *Biogeosciences*, *11*, 7137–7158.
Sawicz, K., T. Wagener, M. Sivapalan, P. A. Troch, and G. Carrillo (2011), Catchment classification: Empirical analysis of hydrologic similarity based on catchment function in the eastern USA, *Hydrol. Earth Syst. Sci.*, *15*, 2895–2911.
Schaake, J. C., V. I. Koren, Q. Y. Duan, K. Mitchell, and F. Chen (1996), Simple water balance model for estimating runoff at different spatial and temporal scales, *J. Geophys. Res.*, *101*(D3), 7461–7475.
Sellers, P. J. (1985), Canopy reflectance, photosynthesis and transpiration, *Int. J. Remote Sens.*, *6*(8), 1335–1372.
Sellers, P. J., M. D. Heiser, and F. G. Hall (1992), Relations between surface conductance and spectral vegetation indices at intermediate (100 m_2 to 15 km_2) length scales, *J. Geophys. Res.*, *97*(D17), 19,033–19,059.

Sellers, P. J., et al. (1997), Modeling the exchanges of energy, water, and carbon between continents and the atmosphere, *Science*, *275*(5299), 502–509.

Shafii, M., and B. A. Tolson (2015), Optimizing hydrological consistency by incorporating hydrological signatures into model calibration objectives, *Water Resour. Res.*, *51*, 3796–3814, doi:10.1002/2014WR016520.

Shamir, E., B. Imam, H. V. Gupta, and S. Sorooshian (2005), Application of temporal streamflow descriptors in hydrologic model parameter estimation, *Water Resour. Res.*, *41*, W06021, doi:10.1029/2004WR003409.

Skamarock, W. C., J. B. Klemp, J. Dudhia, D. O. Gill, D. M. Barker, M. G. Duda, X.-Y. Huang, W. Wang, and J. G. Powers (2008), A description of the Advanced Research WRF version 3, *NCAR Tech. Note NCAR/TN-4751STR*, Natl. Cent. for Atmos. Res., Boulder, Colo.

Sobol', I. M. (1993), Sensitivity analysis for non-linear mathematical models [English translation], *Math. Model. Comput. Exp.*, *1*, 407–414.

Taylor, K. E. (2001), Summarizing multiple aspects of model performance in a single diagram, *J. Geophys. Res.*, *106*(D7), 7183–7192.

Van Werkhoven, K., T. Wagener, P. Reed, and Y. Tang (2008), Characterization of watershed model behavior across a hydroclimatic gradient, *Water Resour. Res.*, *44*, W01429, doi:10.1029/2007WR006271.

Verseghy, D. L. (1991), CLASS—A Canadian land surface scheme for GCMS. I. Soil model, *Int. J. Climatol.*, *11*, 111–133.

Wood, A. W., and D. P. Lettenmaier (2006), A test bed for new seasonal hydrologic forecasting approaches in the western United States, *Bull. Am. Meteorol. Soc.*, *87*, 1699–1712.

Wood, E. F., et al. (2011), Hyperresolution global land surface modeling: Meeting a grand challenge for monitoring Earth's terrestrial water, *Water Resour. Res.*, *47*, W05301, doi:10.1029/2010WR010090.

Xia, Y., et al. (2012), Continental-scale water and energy flux analysis and validation for the North American Land Data Assimilation System project phase 2 (NLDAS-2): 1. Intercomparison and application of model products, *J. Geophys. Res.*, *117*, D03109, doi:10.1029/2011JD016048.

Yang, R., and M. Friedl (2003), Modeling the effects of three-dimensional vegetation structure on surface radiation and energy balance in boreal forests, *J. Geophys. Res.*, *108*(D16), 8615, doi:10.1029/2002JD003109.

Yang, Z. L., et al. (2011), The community Noah land surface model with multiparameterization options (Noah-MP): 2. Evaluation over global river basins, *J. Geophys. Res.*, *116*, D12110, doi:10.1029/2010JD015140.